THE ASTROPHYSICAL JOURNAL, 302:536–563, 1986 March 15

A DISTANCE SCALE FROM THE INFRARED MAGNITUDE/H I VELOCITY-WIDTH RELATION. V. DISTANCE MODULI TO 10 GALAXY CLUSTERS, AND POSITIVE DETECTION OF BULK SUPERCLUSTER MOTION TOWARD THE MICROWAVE ANISOTROPY

M. AARONSON[1,2]
Steward Observatory, University of Arizona
G. BOTHUN[1,2] AND J. MOULD[1,2]
Palomar Observatory, California Institute of Technology
J. HUCHRA[1,2]
Harvard-Smithsonian Center for Astrophysics
R. A. SCHOMMER[1,2]
Rutgers University
AND
M. E. CORNELL
Steward Observatory, University of Arizona
Received 1985 May 21; accepted 1985 September 13

ABSTRACT

In this paper we utilize the excellent relation between infrared magnitudes and 21 cm velocity widths to derive relative distance moduli to 10 nearby galaxy clusters. Our sample contains a wide variety of cluster types, ranging in redshift from Pegasus at $V \sim 4000$ km s^{-1} up to Hercules at $V \sim 11{,}000$ km s^{-1}, and also includes the Pisces, A400, A539, Cancer, A1367, Coma, Z74-23, and A2634/66 systems.

Considerable attention is devoted to a problem involving the differing surface brightness properties of the cluster samples. Specifically, the surface brightnesses of galaxies in the higher redshift clusters are in the mean found to be lower than in nearby clusters *at fixed velocity width*. To investigate whether this effect is caused by galaxy diameter errors, we have secured charged coupled device (CCD) imaging for over a hundred cluster spirals. The true isophotal radii derived from these data do indeed systematically disagree with our previously employed eye-measured diameters, but by an amount that only partially accounts for the surface brightness variations. The remaining differences are attributed to a real selection effect which severely biases distances estimated from the magnitude/surface brightness relation toward smaller values. We demonstrate, however, that the effect is likely to bias distances obtained from the IR/H I relation toward *larger* values, but the amount of bias is minimal with the present data set and is ignored.

Our cluster sample suffers from one additional selection bias related to the nonlinear shape of the IR/H I relation. To account for this behavior we adopt a quadratic form of the relation. Several other possible sample biases, including the Malmquist effect, are considered and dismissed.

The final Hubble ratios, based on newly derived cluster redshifts, are found to exhibit a scatter considerably larger than the formal errors, which we show arises from the presence of a Local Group velocity component. Formal solution for the motion yields $V = 780 \pm 188$ km s^{-1} toward $l = 255° \pm 17°$ and $b = 18° \pm 13°$. This vector agrees well in both magnitude and direction with the 3 K dipole anisotropy, for which $V = 600 \pm 30$ km s^{-1} toward $l = 268° \pm 3°$ and $b = 27° \pm 3°$, a velocity which is in turn roughly double the known Local Group motion in the Local Supercluster. Hence, we conclude that the motion giving rise to the 3 K dipole has been positively detected, and consists of two principal components having comparable size; these are Local Group motion within the Supercluster, primarily toward Virgo, and bulk Supercluster motion as a whole, in a direction lying close to that of our next nearest neighbor supercluster, Hydra-Centaurus.

By comparing our cluster Hubble ratios with that of Virgo, a new estimate of the Virgocentric motion is also derived. The result, $\Delta V \sim 300$ km s^{-1}, is in excellent agreement with our earlier analysis of the Local Supercluster velocity field. After correcting Virgo and our 10-cluster sample for all appropriate streaming effects, we obtain a velocity-distance relation linear to within the measurement errors. This finding constrains supercluster-supercluster interactions to be less than 500 km s^{-1} in size, a result having important implications with regard to the formation of galaxies and the distribution of large-scale mass in the universe.

Our data also suggest that environmental effects play little part in application of the IR/H I technique. Unfortunately, derivation of an absolute calibration continues to be frustrated by the present-day confusing state of nearby galaxy distances. A "best guess" calibration based on recent infrared and CCD observations of extragalactic Cepheids yields a global value for the Hubble constant of $H_0 = 90$ km s^{-1} Mpc^{-1}, but proper calibration of the method remains a fundamental task for the Hubble Space Telescope.

Subject headings: cosmic background radiation — cosmology — galaxies: clustering — galaxies: internal motions — galaxies: photometry

[1] Visiting Astronomer, Kitt Peak National Observatory. KPNO is a division of National Optical Astronomy Observatories, operated by the Association of Universities for Research in Astronomy, Inc., under contract to the National Science Foundation.

[2] Visiting Scientist, Arecibo Observatory, National Astronomy and Ionosphere Center. NAIC is operated by Cornell University under contract to the National Science Foundation.

I. INTRODUCTION

It is now widely recognized that the Local Group deviates from uniform Hubble flow as a result of gravitational perturbation caused by the Virgo Cluster mass concentration. This effect must be properly accounted for in any attempt to measure the expansion rate. Two general approaches are available for treating the problem. First, a correction determined from flow studies within the Supercluster can be directly appled to the observed Virgo Hubble ratio (e.g., Aaronson *et al.* 1982*a*, hereafter AHMST). Second, we can jump well beyond the Local Supercluster and measure H_0 for objects which should have minimal flow deviations. It is the aim of this paper to explore the latter alternative, using as a distance indicator the well-established relation between galaxian infrared magnitude and H I velocity width (Aaronson, Huchra, and Mould 1979; Tully and Fisher 1977).

Additional motivation for the study of galaxy distances beyond the Supercluster is provided by observations of the dipole anisotropy in the 3 K microwave background. It now appears that Local Group motion within the Supercluster itself is insufficient to account for the observed effect (e.g., Wilkinson 1984). Identification of the scale size involved in the additional component of motion required is clearly of interest. A natural possibility is that the Local Supercluster itself partakes of bulk motion with respect to other nearby massive clusters. If so, the signature of such motion ought to be reflected in the observed Hubble ratios of the latter.

A first attempt to investigate the IR/H I relation beyond the Local Supercluster was presented by Aaronson *et al.* (1980, hereafter Paper III). These authors studied a small number of galaxies in only four clusters, but nevertheless found a significantly larger Hubble ratio than was seen for Virgo, implying a Virgocentric velocity of $\sim 480 \pm 75$ km s^{-1}. This amount was substantially larger than the value of $\sim 300 \pm 40$ km s^{-1} found subsequently by AHMST on applying the IR/H I relation to the velocity field of the Local Supercluster. Following that effort, Aaronson and Mould (1983, hereafter Paper IV) used the Local Supercluster sample to make a careful study of the instrinsic properties of the IR/H I relation. In particular, the method was found to have a typical observational scatter of only ~ 0.45 mag, with little dependence on morphological type (although the latter point remains controversial). Nonlinearity in the IR/H I relation was also identified.

In this paper we focus our attention on 10 nearby galaxy clusters, ranging in mean redshift from 4000 to 11,000 km s^{-1}. We emphasize that working in such clusters provides an effective way to combat bias inherent in magnitude-limited samples, because the galaxies in each cluster are generally all at the same distance. The variety of cluster types employed also allows us to reexamine the question of environmental dependence.

The outline of the paper is as follows. The basic observations are presented in § II; the discussion here is kept short, since Bothun *et al.* (1985*a*) have already given a full description of the measurements and data reduction. In § III we discuss a problem originally identified by van den Bergh (1981) involving mean surface brightness variations in the cluster samples. The extent to which this effect is accounted for by galaxy diameter errors is extensively investigated in § IV. The cluster distance moduli and Hubble ratios are derived in § V, after first considering a number of potential biases in the data. In § VI we carry out a variety of solar motion solutions with respect to the reference frame of the clusters. The value of the Hubble constant is discussed in § VII. Finally, our conclusions are briefly summarized in § VIII. (An appendix is also provided containing several technical details.)

II. OBSERVATIONS

The positions and mean redshifts of our 10-cluster sample are given in Table 1. The list encompasses virtually all the well-known nearby clusters within Arecibo's declination limits, and spans a wide variety of cluster types. This range includes at one limit highly concentrated, spiral-poor clusters such as Coma (18% spirals) and Abell 400 (36% spirals), and at the other extreme irregular, spiral rich clusters such as Pegasus (59% spirals) and Cancer (71% spirals) (see Bothun *et al.* 1985*a*, Table 1).

Two sets of mean redshifts are given in Table 1. The first is based on newly derived values calculated from Huchra's (1985) redshift catalog using the search radii and velocity ranges listed in the table. The second set lists the mean H I velocities of the galaxies used in this paper to derive distances. In general, the

TABLE 1

CLUSTER VELOCITIES

Name	Position (1950) R.A.	Position (1950) Decl.	Search Radius	Search Velocities (km s^{-1})	V[a] (km s^{-1})	N	IR/H I Sample V[a] (km s^{-1})	IR/H I Sample N
Pisces	1h00m	+30°00′	4°	4200–6400	5274 ± 58	54	5274 ± 97	20
A400	2 55	5 50	3	5400–8800	7154 ± 90	52[b]	7855 ± 135	7
A539	5 14	6 23	3	6600–10200	8561 ± 123	40	8536 ± 102	9
Cancer	8 18	21 14	4	3200–7000	4790 ± 89	87	4789 ± 186	22
A1367	11 42	20 07	3	4600–8800	6427 ± 73	109	6486 ± 142	20
Coma	12 57.4	28 15	3	5000–8800	6931 ± 45	292[c]	7310 ± 132	13
Z74-23	14 00	9 34	3	4000–7400	6025 ± 153	38	5939 ± 270	13
Hercules	16 03	17 56	3	8400–14400	11077 ± 97	142	10733 ± 244	11
Pegasus	23 18	7 55	4	2600–5400	4078 ± 78	62[d]	4275 ± 132	22
A2634/66	23 40	24 00	4	6800–10200	8783 ± 115	55	8694 ± 215	11
Virgo	12 28.3	12 40	6	−600–3000	1073 ± 38	362	1064 ± 168	16

[a] Corrected for motion according to 300 sin l cos b, here and in following tables.

[b] Apparent foreground objects U2364 and U2509 eliminated.

[c] Clump at $V \sim 4900$ in foreground, based on IR/H I distances to N4738, U7754, and Z160139; N5065 and U8392 are also apparent foreground objects (but out of area search range regardless).

[d] Foreground pair N7537 and N7541 eliminated.

agreement between the two sets is within the errors, indicating that with the present, limited base we are fairly sampling the cluster distances. This is an important point, because the mean cluster velocities are heavily weighted by the high concentration of galaxies in the cluster cores, whereas our H I sample here is more weighted by objects in the outer periphery, where gas-rich spirals are more commonly found. The one substantial disagreement is with Abell 400, where apparently the present sample lies at a considerably higher mean velocity than the cluster as a whole. A clue to the underlying reason for this discrepancy is provided by an ongoing study of the region being conducted by T. Beers (1985), which appears to show that A400 is a two-component system containing a foreground cluster proper consisting mostly of early-type galaxies, and a background supercluster dominated by spirals.

Also included in Table 1 is a newly determined redshift for the Virgo cluster of 1073 ± 38 km s^{-1} from Huchra (1984). This value is 54 km s^{-1} larger than, and supersedes, the Virgo redshift of 1019 ± 51 of Mould, Aaronson, and Huchra (1980, hereafter Paper II) employed in our previous work. The increase is due partly to a near doubling of the sample size, and partly to a more appropriate upper search cutoff of 3000 km s^{-1} rather than 2500 km s^{-1}. Note that all of the velocities in Table 1 are adjusted to the velocity centroid of the Local Group using the standard IAU correction 300 sin l cos b. We will explore later the effects of employing the alternative correction of Yahil, Sandage, and Tammann (1977, hereafter YST).

Table 2 presents the fundamental observational material on which this paper is based. Column (1) gives the galaxy name (following the ordering convention of Bothun *et al.* 1985*a*). Column (2) lists the inclination, calculated from axial ratios using equation (4) of Aaronson, Mould, and Huchra (1980, hereafter Paper I), which includes a 3° additive term. The velocity width at the 20% level (defined as in Paper I), corrected for inclination effect and redshift according to equation (1) of Paper III is given in column (3). The 21 cm radial velocity is shown in column (4), where again a correction of 300 sin l cos b has been employed. In column (5) we give the H (1.6 μm) magnitude at $\log (A/D_1) = -0.5$, corrected for Galactic reddening and $(1 + z)^4$ surface brightness effect following equation (7) of Paper III. Listed in column (6) is the diameter of the 25th mag B isophote (in logarithmic units of 0.'1) reduced to a face-on value and corrected for Galactic extinction. As discussed in Paper I, $\log D_1$ is essentially (though not exactly) the same as $\log D_0$ in the *Second Reference Catalogue of Bright Galaxies* (de Vaucouleurs, de Vaucouleurs, and Corwin 1976, hereafter RC2). While the inclination and extinction corrections to the diameters, though minor in the long run, have been the subject of some debate, a recent study by Tully and Fouqué (1985) has largely confirmed the basic RC2 procedures we have employed. Finally, the surface brightness $\Sigma_H \equiv H^c_{-0.5} + 5 \log D_1$ is presented in column (7). The next three columns in Table 1 are revised values of $\log D_1$, $H^c_{-0.5}$, and Σ_H discussed further below. The quantities in columns (2)–(5) are in general directly adopted from Table 7 of Bothun *et al.* (1985*a*), with minor corrections applied in a few instances. Note that all of the H I data come from Arecibo, while the vast majority of IR photometry was obtained at Kitt Peak National Observatory, primarily using the Harvard-Smithsonian InSb detector; a small fraction of the photometry was secured with the Hale 5 m telescope.

Our selection criteria remain the same as in earlier papers in this series: the only accepted galaxies are those having (1) $i \geq 45°$, (2) no obvious morphological peculiarities, and (3) high signal-to-noise level H I profiles. For the most part, every cluster member listed with an H I width in Table 7 of Bothun *et al.* (1985*a*) is included here. Unfortunately, the operational definition of our third criterion remains somewhat subjective, and in a full reconsideration of the profiles we have dropped a few of the Table 7 widths and added a few others. Also not included from that table are foreground or background systems, i.e. those outside the search velocity ranges in Table 1 here, and a few objects which failed to meet our other two selection criteria. As in earlier papers, we again forgo the very small correction for instrumental resolution, and possible small but uncertain corrections for internal extinction or velocity dispersion effects. However, in a few cases of low signal-to-noise ratio (noted in Table 2), we have derived 20% line widths from the 50% values by multiplying the latter by 1.1 (see Paper I).

We note in passing that H I line widths are available from other observers both for some of the galaxies here and for other member galaxies of our clusters (e.g., Chincarini, Giovanelli, and Haynes 1979 for Z74-23; Chincarini *et al.* 1983 and Chincarini, Giovanelli, and Haynes 1983 for A1367 and Coma; Giovanelli, Chincarini, and Haynes 1981 for Hercules; and Richter and Huchtmeier 1982 for Pegasus). We had hoped to incorporate these data into the analysis. Unfortunately, a detailed comparison of our line widths with those from elsewhere does not yield entirely satisfactory results, showing excellent agreement in some cases but poor correspondence in others, possibly as a result of differing details in the reduction procedures. The data set in this paper has been reduced in a completely uniform manner using a method which, as discussed further below, Lewis (1983) has demonstrated to be very stable against noise effects. For this reason, we have decided against the use at present of other line widths.

III. ISOPHOTAL DIAMETERS AND THE SURFACE BRIGHTNESS PROBLEM

Evidence that the isophotal diameters in Paper III might be affected by systematic scale errors first emerged in a study by van den Bergh (1981), who attempted to use a relation between H-magnitude and infrared surface brightness Σ_H to derive relative distances. His results appeared to indicate an implausibly large value for Virgocentric motion of the Local Group. A careful examination of the situation revealed that while the (H, Σ_H) and IR/H I relations yielded consistent moduli for two of the four distant groupings studied in Paper III (Pegasus and Cancer), highly discrepant values were obtained for the other two groupings (Z74-23 and Perseus). We found a similar dichotomy (as did Kraan-Korteweg 1983 and Bosma 1985) upon examining the surface brightness/velocity-width $[(\Sigma_H, \Delta V)]$ diagram. In the following discussion, we shall emphasize this latter relation because of the obvious advantage that both quantities involved are distance independent.

Although (as discussed in the next section) there are several possibilities, the most natural cause of the above problems seems to rest with the isophotal diameters. For several technical reasons explained in Paper I, our adopted H-magnitudes are tied to the blue diameters of the RC2. For virtually all of the distant cluster galaxies, these diameters were originally obtained from Nilson (1973, hereafter UGC) or in a few instances measured by one of us (M. A.) on glass copies of the Palomar Sky Survey at Kitt Peak, and in either case then

TABLE 2

CLUSTER DATA

Name	i	$\Delta V^c_{20}(0)$ (km s^{-1})	V (km s^{-1})	Old $H^c_{-0.5}$ (mag)	Old log D_1	Old Σ_H (mag)	Revised $H^c_{-0.5}$ (mag)	Revised log D_1	Revised Σ_H (mag)	$H^{c,abs}_{-0.5}$ (mag)	m-M (mag)	r (Mpc)	V/r (km s^{-1} Mpc^{-1})	Notes
1	2	3	4	5	6	7	8	9	10	11	12	13	14	15
Pisces:														
N295	69	499	5666	10.05	1.27	16.40	10.11	(1.23)	16.26	-22.97	33.08	41	137	
N296	81	275	5861	13.14	0.99	18.09	13.33	(0.92)	17.93	-20.34	33.67	54	108	
N338	72	570	4982	9.98	1.21	16.03	10.02	(1.16)	15.82	-23.42	33.44	49	102	
N444	84	293	5034	12.45	1.19	18.40	12.62	(1.10)	18.12	-20.67	33.29	46	111	
N452	69	551	5156	9.98	1.35	16.73	10.01	1.31	16.56	-23.31	33.32	46	112	
N496	61	365	6197	11.74	1.19	17.69	11.89	(1.14)	17.59	-21.72	33.61	53	118	1
N536	65	624	5383	9.75	1.52	17.35	9.82	1.45	17.07	-23.70	33.52	51	107	
N582	79	467	4542	10.56	1.24	16.76	10.66	(1.19)	16.61	-22.73	33.39	48	95	
U501	90	408	5299	11.90	1.12	17.50	12.06	(1.02)	17.16	-22.20	34.26	71	75	
U525	56	300	5146	12.76	1.20	18.76	12.95	1.12	18.55	-20.79	33.74	56	92	
U540	62	313	5192	12.56	0.83	16.71	12.46	0.87	16.81	-21.00	33.46	49	106	
U556	56	492	4836	11.01	1.06	16.31	11.07	0.98	15.97	-22.92	33.99	63	77	
U557	66	298	4708	13.16	1.01	18.21	13.18	0.99	18.13	-20.76	33.94	61	77	2
U575	90	315	4876	12.91	0.89	17.36	13.19	(0.79)	17.14	-21.03	34.22	70	70	
U633	82	416	5783	11.62	1.11	17.17	11.72	1.04	16.92	-22.28	34.00	63	92	
U679	77	209	5286	14.78	1.01	19.83	15.15	0.92	19.75	-18.80	33.95	62	86	2
U732	61	341	5645	11.83	1.19	17.78	12.00	(1.12)	17.60	-21.41	33.41	48	117	
U841	81	306	5773	12.43	1.10	17.93	12.60	(1.02)	17.70	-20.89	33.49	50	116	
U987	76	444	4856	10.42	1.31	16.97	10.63	1.15	16.38	-22.53	33.16	43	113	
U1066	81	178	5268	14.74	1.03	19.89	14.99	(0.90)	19.49	-17.79	32.78	36	146	2
A400:														
U2285	72	332	8393	12.64	1.07	17.99	12.75	(1.02)	17.85	-21.28	34.03	64	131	
U2367	73	634	7426	10.55	1.23	16.70	10.59	1.20	16.59	-23.74	34.33	74	101	
U2375	78	462	7647	11.66	0.96	16.46	11.81	(0.92)	16.41	-22.69	34.50	79	96	
U2405	62	515	7748	11.59	1.21	17.64	11.85	1.10	17.35	-23.08	34.93	97	80	2
U2414	85	430	8298	12.63	0.96	17.43	12.69	(0.92)	17.29	-22.41	35.10	105	79	2
U2415	72	385	7809	12.33	0.98	17.23	12.45	(0.94)	17.15	-21.95	34.40	76	103	
U2454	76	397	7667	12.37	1.03	17.52	12.44	1.00	17.44	-22.08	34.52	80	96	
A539:														
U3219	67	342	8419	13.03	1.11	18.58	13.30	(0.98)	18.20	-21.42	34.72	88	96	
U3220	53	352	8446	13.55	1.05	18.80	13.79	(0.94)	18.49	-21.55	35.34	117	72	
U3236	72	445	8440	12.51	1.01	17.56	12.77	(0.90)	17.27	-22.54	35.31	116	73	
U3248	63	510	8860	11.35	1.23	17.50	11.55	(1.11)	17.10	-23.05	34.60	83	107	
U3269	55	391	8871	12.10	1.00	17.10	12.41	0.87	16.76	-22.02	34.43	77	116	
U3270	70	396	8563	12.58	0.97	17.43	12.78	(0.87)	17.13	-22.07	34.85	93	92	
U3275	84	567	7901	11.62	1.16	17.42	11.79	(1.01)	16.84	-23.40	35.19	109	72	
Z421011	73	406	8841	12.21	0.96	17.01	12.35	0.89	16.80	-22.17	34.52	80	110	
Z421030	70	496	8487	12.05	0.86	16.35	12.05	0.86	16.35	-22.95	35.00	100	85	

TABLE 2—*Continued*

Name	i	$\Delta V^c_{20}(0)$ (km s^{-1})	V (km s^{-1})	Old $H^c_{-0.5}$ (mag)	Old log D_1	Old Σ_H (mag)	Revised $H^c_{-0.5}$ (mag)	Revised log D_1	Revised Σ_H (mag)	$H^{c,abs}_{-0.5}$ (mag)	m-M (mag)	r (Mpc)	V/r (km s^{-1} Mpc^{-1})	Notes
1	2	3	4	5	6	7	8	9	10	11	12	13	14	15
Cancer:														
I2288(E)	66	261	4514	13.97	0.73	17.62	13.93	(0.76)	17.73	-20.07	34.00	63	72	2
I2308(F)	68	378	5623	12.65	0.76	16.45	12.63	(0.77)	16.48	-21.87	34.50	79	71	3
I2348(B)	67	388	5869	12.52	0.88	16.92	12.90	0.80	16.90	-21.98	34.88	95	62	
N2565(D)	70	465	3489	9.85	1.21	15.90	9.87	1.20	15.87	-22.71	32.58	33	106	
N2570(B)	60	355	6439	12.23	1.09	17.68	12.33	(1.03)	17.48	-21.59	33.92	61	106	
N2596(-)	70	471	5808	11.33	1.12	16.93	11.37	1.10	16.87	-22.76	34.13	67	87	
U4299(E)	90	411	4195	10.94	1.17	16.79	10.96	1.16	16.76	-22.23	33.19	43	97	
U4329(D)	55	347	3714	11.49	1.36	18.29	11.91	1.17	17.76	-21.49	33.40	48	78	4
U4361(D)	71	220	3645	13.70	1.02	18.80	13.88	(0.96)	18.68	-19.10	32.98	39	92	
U4386(A)	80	506	4547	10.61	1.18	16.51	10.60	1.19	16.55	-23.02	33.62	53	86	
U4399(A)	72	263	4396	13.00	0.97	17.85	13.09	(0.93)	17.74	-20.11	33.20	44	101	
U4400(A)	90	250	4293	13.93	1.10	19.43	14.24	0.96	19.04	-19.83	34.07	65	66	
U4405(C)	79	508	5559	10.91	1.08	16.31	11.01	(1.01)	16.06	-23.03	34.04	64	86	2,5
U4416(C)	73	426	5426	10.91	1.31	17.46	11.03	1.24	17.23	-22.37	33.40	48	113	
U4424(A?)	82	247	4336	14.03	1.01	19.08	13.91	1.05	19.16	-19.76	33.67	54	80	6
U4446(B)	90	348	5897	12.56	0.96	17.46	12.83	(0.89)	17.28	-21.50	34.33	74	80	
Z119044(D)	58	191	3405	14.46	0.90	18.96	14.53	(0.87)	18.88	-18.24	32.77	36	95	
Z119051(A)	59	290	4928	13.53	0.99	18.48	13.62	(0.95)	18.37	-20.62	34.24	70	70	
Z119053(A)	50	280	4749	12.93	0.80	16.93	12.90	(0.82)	17.00	-20.44	33.34	47	102	
Z119066(E)	45	331	4045	12.55	0.90	17.05	12.31	1.00	17.31	-21.27	33.58	52	78	
Z119095(C)	90	428	5286	12.81	0.89	17.26	12.91	(0.85)	17.16	-22.39	35.30	115	46	
Z119107(C)	79	374	5193	13.02	0.88	17.42	13.07	(0.85)	17.32	-21.82	34.89	95	55	
A1367:														
N3697	78	552	6187	10.80	1.28	17.20	10.85	1.25	17.10	-23.32	34.17	68	91	
N3840	50	380	7298	11.62	1.03	16.77	11.66	0.99	16.61	-21.89	33.55	51	142	
N3861	56	586	5024	10.47	1.33	17.12	10.49	1.31	17.04	-23.51	34.00	63	80	
N3951	63	472	6408	11.31	1.04	16.51	11.39	1.00	16.39	-22.77	34.16	68	94	
U6583	62	428	6112	11.88	0.83	16.03	11.79	(0.87)	16.14	-22.39	34.18	69	89	
U6686	90	419	6458	11.16	1.31	17.71	11.22	1.24	17.42	-22.30	33.52	51	127	
U6837	90	368	5901	13.21	0.88	17.61	13.42	(0.83)	17.57	-21.75	35.17	108	54	
U6891	85	399	6703	11.88	1.10	17.38	12.22	1.03	17.37	-22.10	34.32	73	92	
Z097005	67	302	6045	13.28	0.87	17.63	13.32	(0.85)	17.57	-20.82	34.14	67	90	2,7
Z097033	71	426	7663	12.40	0.85	16.65	12.50	0.80	16.50	-22.37	34.87	94	81	
Z097058	73	299	6653	13.28	0.93	17.93	13.42	(0.90)	17.92	-20.77	34.19	69	96	
Z097062	67	313	7708	13.20	0.87	17.55	13.23	(0.85)	17.48	-21.00	34.23	70	110	.
Z097068	45	485	5889	11.52	1.04	16.72	11.57	1.02	16.67	-22.87	34.44	77	76	
Z097152	75	455	6118	12.12	0.96	16.92	12.24	0.90	16.74	-22.63	34.87	94	65	
Z097180	71	324	6121	14.01	0.85	18.26	14.06	(0.82)	18.16	-21.17	35.23	111	55	
Z097185	72	361	6271	13.04	0.92	17.64	13.12	(0.88)	17.52	-21.67	34.79	91	69	
Z127005	59	350	6800	13.05	0.98	17.95	13.15	(0.94)	17.85	-21.53	34.68	86	79	
Z127049	73	320	6994	12.52	0.93	17.17	12.59	(0.89)	17.04	-21.11	33.70	55	127	
Z127056	77	436	6771	12.17	0.92	16.77	12.26	(0.87)	16.61	-22.46	34.72	88	77	2
Z127082	49	350	6595	12.59	0.91	17.14	12.59	0.91	17.14	-21.53	34.12	67	99	

TABLE 2—*Continued*

Name	i	$\Delta V^c_{20}(0)$ (km s^{-1})	V (km s^{-1})	Old $H^c_{-0.5}$ (mag)	Old log D_1	Old Σ_H (mag)	Revised $H^c_{-0.5}$ (mag)	Revised log D_1	Revised Σ_H (mag)	$H^{c,abs}_{-0.5}$ (mag)	m-M (mag)	r (Mpc)	V/r (km s^{-1} Mpc^{-1})	Notes
1	2	3	4	5	6	7	8	9	10	11	12	13	14	15
Coma:														
I0842	60	458	7285	11.99	1.08	17.39	12.11	1.03	17.26	-22.65	34.76	90	81	
I4088	77	497	7114	11.47	1.13	17.12	11.51	(1.10)	17.01	-22.96	34.47	78	91	
N4966	66	488	7057	11.19	0.96	15.99	11.14	(1.00)	16.14	-22.89	34.03	64	110	
N5081	75	575	6680	11.10	1.24	17.30	11.10	1.24	17.30	-23.45	34.55	81	82	
U7750	72	476	8057	11.61	1.07	16.96	11.66	(1.04)	16.86	-22.80	34.46	78	103	
U7978	60	381	8108	12.33	1.08	17.73	12.37	(1.06)	17.67	-21.91	34.28	72	113	
U8013	78	395	7884	12.87	1.05	18.12	13.00	(1.00)	18.00	-22.06	35.06	103	77	
U8017	74	570	7062	11.30	0.89	15.75	11.28	0.91	15.83	-23.42	34.70	87	81	
U8161	70	412	6682	11.93	0.95	16.68	11.91	0.96	16.71	-22.24	34.15	67	99	
U8195	90	260	7064	13.77	1.01	18.82	13.95	(0.94)	18.65	-20.05	34.00	63	112	
U8244	65	336	7123	13.56	1.06	18.86	13.71	(1.00)	18.71	-21.34	35.05	102	70	
Z130008	45	340	7257	13.32	0.76	17.12	13.23	(0.80)	17.23	-21.39	34.62	84	86	
Z160058	75	381	7657	12.57	0.96	17.37	12.61	0.94	17.31	-21.91	34.52	80	96	
Z74-23:														
N5409	52	451	6237	11.24	1.20	17.24	11.28	1.17	17.13	-22.60	33.88	60	105	
N5416	60	433	6208	11.15	1.14	16.85	11.29	1.08	16.69	-22.44	33.73	56	112	
U8861	70	241	4875	14.08	1.06	19.38	14.34	0.95	19.09	-19.63	33.97	62	78	
U8918	90	334	4070	11.77	1.09	17.22	11.95	0.98	16.85	-21.31	33.26	45	91	
U8927	72	333	7081	13.30	0.98	18.20	13.50	(0.90)	18.00	-21.30	34.80	91	78	
U8948	64	401	5969	11.85	1.12	17.45	12.09	0.97	16.94	-22.12	34.21	70	86	
U8950	90	219	5843	14.45	0.95	19.20	14.96	(0.86)	19.26	-19.08	34.04	64	91	
U8951	80	312	5857	13.87	0.92	18.47	14.04	0.87	18.39	-20.98	35.02	101	58	
U8967	90	385	5611	11.67	1.12	17.27	11.68	1.11	17.23	-21.95	33.63	53	105	
U9023	68	288	7185	13.80	1.02	18.90	14.05	(0.94)	18.75	-20.58	34.63	84	85	
U9027	85	300	6853	13.90	0.88	18.30	14.06	(0.81)	18.11	-20.79	34.85	93	73	
Z074012	78	304	6854	13.82	1.00	18.82	14.00	(0.92)	18.60	-20.86	34.86	94	73	
Z074035	90	244	4558	14.49	0.92	19.09	14.66	(0.84)	18.86	-19.70	34.36	74	61	
Hercules:														
I1173	53	551	10542	12.26	1.03	17.41	12.48	0.91	17.03	-23.31	35.79	144	73	
I1179	46	327	11268	14.02	0.83	18.17	13.88	0.90	18.38	-21.21	35.09	104	108	
N6050	67	417	9700	12.72	0.91	17.27	12.87	(0.82)	16.97	-22.28	35.15	107	90	
U10085	48	420	9832	12.16	1.00	17.16	12.20	0.98	17.10	-22.31	34.51	80	123	
U10190	90	318	11182	14.10	0.88	18.50	14.30	(0.75)	18.05	-21.08	35.38	119	94	
U10195	82	565	10840	11.91	1.12	17.51	12.16	0.99	17.11	-23.39	35.55	129	84	
Z108095	79	362	9513	12.83	0.88	17.23	13.01	(0.81)	17.06	-21.68	34.69	87	110	
Z108098	60	373	12020	13.43	0.86	17.73	13.70	0.75	17.45	-21.81	35.51	127	95	
Z108108	54	370	10741	12.73	0.91	17.28	13.04	0.74	16.74	-21.78	34.82	92	117	
Z108140	59	544	11716	12.27	0.94	16.97	12.49	(0.86)	16.79	-23.27	35.76	142	83	2
Z108158	81	513	10706	12.26	0.87	16.61	12.40	(0.81)	16.45	-23.07	35.47	124	86	

TABLE 2—*Continued*

Name	i	$\Delta V^c_{20}(0)$ (km s^{-1})	V (km s^{-1})	Old $H^c_{-0.5}$ (mag)	Old log D_1	Old Σ_H (mag)	Revised $H^c_{-0.5}$ (mag)	Revised log D_1	Revised Σ_H (mag)	$H^{c,abs}_{-0.5}$ (mag)	m−M (mag)	r (Mpc)	V/r (km s^{-1} Mpc^{-1})	Notes
1	2	3	4	5	6	7	8	9	10	11	12	13	14	15
Pegasus:														
I1474	66	308	3665	11.80	1.00	16.80	11.84	0.98	16.74	-20.92	32.76	36	103	
I5309	70	337	4386	11.61	1.11	17.16	11.66	1.08	17.06	-21.35	33.01	40	110	
N7536	72	367	4927	11.09	1.26	17.39	11.22	(1.21)	17.27	-21.74	32.96	39	126	
N7591	68	463	5146	10.32	1.21	16.37	10.39	1.17	16.24	-22.70	33.09	41	124	
N7631	66	412	3941	10.71	1.22	16.81	10.80	1.18	16.70	-22.24	33.04	40	97	
U12304	90	315	3659	11.60	1.01	16.65	11.40	1.08	16.80	-21.03	32.43	31	119	
U12361	70	201	3206	14.38	0.95	19.13	13.45	0.92	18.05	-18.56	32.01	25	127	
U12370	82	280	5104	12.80	1.05	18.05	12.74	1.08	18.14	-20.44	33.18	43	118	
U12382	90	303	3716	12.72	0.96	17.52	12.82	(0.91)	17.37	-20.84	33.66	54	69	2
U12423	90	526	5046	10.82	1.40	17.82	10.87	1.38	17.77	-23.15	34.02	64	79	
U12451	81	212	3825	13.65	1.09	19.10	13.70	1.07	19.05	-18.88	32.58	33	116	
U12467	79	252	3696	13.35	1.07	18.70	13.38	1.06	18.68	-19.87	33.25	45	83	
U12494	74	260	4376	13.42	1.09	18.87	13.40	1.10	18.90	-20.05	33.45	49	89	
U12497	83	184	3957	13.77	0.94	18.47	13.72	0.96	18.52	-18.01	31.73	22	179	
U12547	62	267	5299	12.97	1.04	18.17	13.05	(1.01)	18.10	-20.19	33.24	44	119	
U12555	79	257	5101	14.11	0.95	18.86	14.19	(0.91)	18.74	-19.98	34.17	68	75	
U12561	82	229	3944	13.88	1.11	19.43	14.10	1.01	19.15	-19.34	33.44	49	81	
U12562	82	197	4046	14.14	1.00	19.14	14.25	(0.95)	19.00	-18.44	32.69	34	117	
Z406031	77	249	4927	13.63	0.92	18.23	13.82	0.79	17.77	-19.81	33.63	53	93	2
Z406079	65	210	4084	13.29	1.04	18.49	13.29	1.04	18.49	-18.83	32.12	26	154	
Z406082	72	243	4195	12.38	0.84	16.58	12.42	(0.82)	16.52	-19.67	32.09	26	160	
Z406086	84	227	3796	13.41	0.87	17.76	13.48	(0.84)	17.68	-19.28	32.76	36	106	
A2634/66:														
N7747	72	615	7933	10.78	1.16	16.58	10.85	(1.12)	16.45	-23.65	34.50	80	100	
U12631	80	484	9430	11.72	0.94	16.42	11.74	(0.92)	16.34	-22.86	34.60	83	113	
U12678	90	545	9198	11.95	0.96	16.75	12.05	(0.90)	16.55	-23.27	35.32	116	79	
U12701	90	376	9104	12.81	0.89	17.26	12.99	(0.81)	17.04	-21.85	34.84	93	98	
U12721	70	448	7849	11.49	1.12	17.09	11.52	1.10	17.02	-22.57	34.09	66	119	
U12746	90	486	7678	11.62	1.02	16.72	11.70	(0.97)	16.55	-22.88	34.58	82	93	
U12755	56	628	9033	11.07	1.18	16.97	11.18	(1.12)	16.78	-23.72	34.90	95	95	
U12855	62	533	8109	11.45	1.11	17.00	11.50	(1.08)	16.90	-23.20	34.70	87	93	2
Z476112	66	548	9645	11.52	0.92	16.12	11.63	(0.88)	16.03	-23.29	34.92	96	100	
Z477024	65	355	8369	12.62	0.85	16.87	12.68	(0.82)	16.78	-21.59	34.27	72	117	
Z498012	73	413	9281	12.19	0.94	16.89	12.23	(0.92)	16.83	-22.25	34.48	79	118	

NOTES.—(1) 21 cm data adopted from Paper III. (2) Velocity width determined from 1.1 × ΔV_{50}. (3) Listed as Z89006 by Bothun *et al.* 1985*a*. (4) Velocity revised from Bothun *et al.* 1985*a*. (5) Hump on profile edge. (6) Bothun *et al.* 1983 did not assign this galaxy to a subgroup; we have tentatively assigned it to group A. (7) Baseline problem in 21 cm data.

TABLE 3

MEAN RESIDUALS ABOUT THE SURFACE BRIGHTNESS/VELOCITY-WIDTH RELATION

		$\langle \Sigma^{obs} - \Sigma^{pred} \rangle$ (mag)	
CLUSTER	*N*	POSS Diameters	GASP Diameters
Virgo	16	-0.17 ± 0.13	...
Ursa Major	24	-0.08 ± 0.13	...
Pisces	20	0.30 ± 0.12	0.08 ± 0.11
A400	7	0.56 ± 0.20	0.44 ± 0.17
A539	9	0.71 ± 0.21	0.40 ± 0.17
Cancer	22	0.02 ± 0.12	-0.07 ± 0.10
A1367	20	0.17 ± 0.12	0.08 ± 0.11
Coma	13	0.44 ± 0.17	0.40 ± 0.15
Z74-23	13	0.49 ± 0.10	0.30 ± 0.11
Hercules	11	0.60 ± 0.15	0.35 ± 0.15
Pegasus	22	-0.16 ± 0.16	-0.28 ± 0.16
A2634/66	11	0.35 ± 0.16	0.23 ± 0.15

transformed to the RC2 system, giving the diameter of the 25th mag isophote. Two disturbing aspects of this procedure are that, first, the diameters are always measured by eye, and, second, the RC2 transformation prescription which we have followed is derived from large galaxies, and may not be at all reliable in the smaller size regime of the cluster objects. These diameter problems were extensively discussed in Paper III, where a variety of tests were performed in search of potential scale errors, though with negative results.

The cluster observations accumulated here allow us now to examine more fully the nature of the (Σ_H, ΔV) relation. To define the fiducial of the relation, we employ the 308 member Local Supercluster galaxy sample of Aaronson *et al.* (1982*b*). A mean least-squares fit to those data (i.e., a fit obtained by treating first one quantity and then the other as the independent variable, and averaging the results) yields the following expression:

$$\Sigma_H = 17.72(\pm 0.61) - 6.89(\pm 0.23)[\log(\Delta V) - 2.5] . \quad (1)$$

We next compare the (Σ, ΔV) relations for our distant sample by forming for each cluster the mean quantity $\langle \Sigma_H^{obs} - \Sigma_H^{pred} \rangle$, where Σ_H^{obs} is taken from column (7) of Table 2, and Σ_H^{pred} is calculated by simply substituting the velocity width from column (3) of Table 2 in equation (1) above. The results are listed in Table 3 and plotted in Figure 1*a*, where we have also included the Virgo and Ursa Major clusters (which form a small subset of the 308 member nearby sample).

A disturbingly strong correlation is evident in Figure 1*a* between mean cluster surface brightness residual and radial velocity. Since our cluster morphology does not relate in any obvious fashion to redshift, the most straightforward interpretation of Figure 1*a* again involves a potential problem with the observables, and most probably the diameters. Motivated by a preliminary version of these findings, we began several years

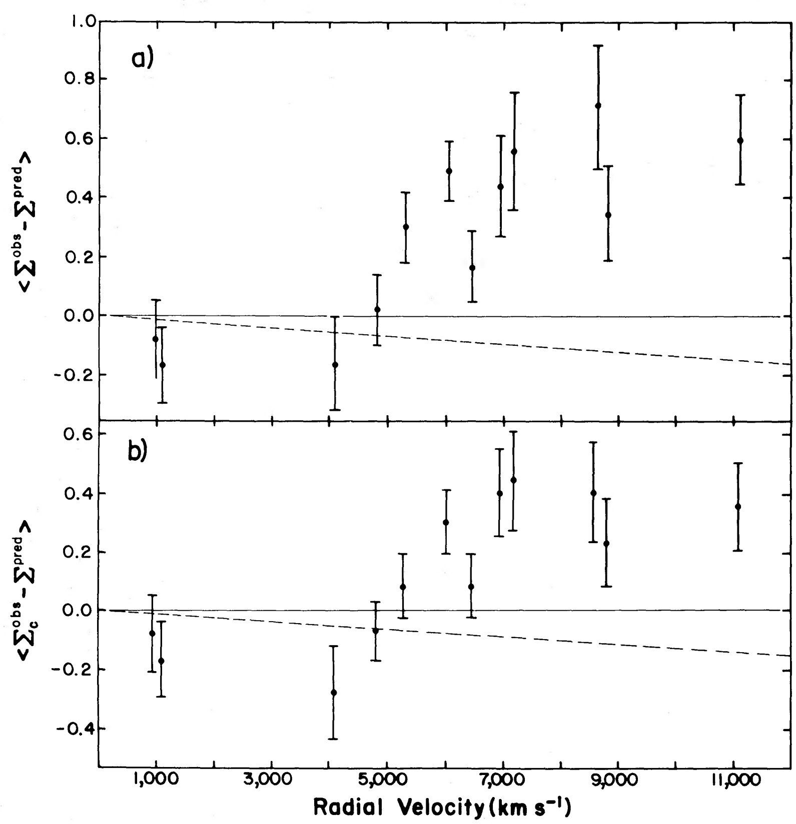

FIG. 1.—Mean difference between observed and predicted surface brightnesses for the sample galaxies in 12 clusters. Here Σ^{obs} ($\equiv H^c_{-0.5} + 5 \log D_1$) is a hybrid quantity involving infrared *H* (1.6 μm) magnitudes but optically measured blue diameters. Σ^{pred} is determined from the velocity width ΔV and the mean (Σ, ΔV) relation defined by 308 galaxies in the Local Supercluster from Aaronson *et al.* (1982*b*). In (*a*) we have used our "old" diameter values for the 10 distant clusters; these are derived from eye measures using Palomar Observatory Sky Survey photographs. In (*b*) we employ revised diameters based on CCD imaging work, which partially diminishes the trend with redshift. The dashed lines in both panels show the expected $(1 + z)^4$ behavior that arises from cosmological expansion. Note that while our definition of $H^c_{-0.5}$ explicitly accounts for this effect, it still enters into Σ because of the 5 log D_1 diameter term (see Paper III).

ago a program of cluster spiral surface photometry, with the explicit purpose of checking our adopted isophotal diameters. The results of this effort, which has considerably delayed our analysis of the cluster observations, are discussed in the next section.

IV. REVISED ISOPHOTAL DIAMETERS AND RECONSIDERATION OF THE SURFACE BRIGHTNESS PROBLEM

Over a 2 year period (mid-1982 to mid-1984), the Kitt Peak No. 1 0.9 m telescope and charge coupled device (CCD) camera were used to secure images of spiral members of our 10-cluster sample. About 250 objects were observed in the R band, and some 150 of these were observed in the B band, where the 15 minute exposure times enabled us to reach well below the 25th magnitude per square second of arc level corresponding to the RC2 system.

A majority of the blue frames have now been reduced using the surface brightness program GASP. Details of this package are available from its author, M. Cawson (now at Steward Observatory). The major fraction of data was processed on the VMS VAX 11/750 at Kitt Peak, while a smaller portion was analyzed on a VMS VAX at Caltech. A full discussion of this work will be presented by Cornell *et al.* (1985). Briefly, elliptical isophotes were fitted to the data for each galaxy, allowing the ellipticity, position angle, and center of each ellipse to vary with radius. The major-axis surface brightness profile thereby determined was calibrated using the multiaperture B band photoelectric photometry of Bothun *et al.* (1985*a*), after which the diameter at the 25th magnitude isophote could be read off.

With these results in hand, a comparison of true isophotal diameters with the UGC diameters transformed to the RC2 system could then be made. In brief, *we found that for small galaxies* ($D < 1\rlap{.}'5$), *the transformed UGC diameters overestimate galaxy size by* $\sim 12\%$ *in the mean.* A consequence of this fact is that the $H^c_{-0.5}$ values derived using these diameters will themselves be overestimated by ~ 0.1 mag, and subsequent distances will thus be underestimated.

The diameter error $\Delta(\log D)$ ($\equiv \log D_{\rm GASP} - \log D_{\rm UGC}$, $D_{\rm UGC}$ being UGC diameters transformed to the RC2 system) was not found to be correlated with galaxy size $\log D$ itself, and therefore no relation was seen between $\Delta(\log D)$ and cluster redshift. For instance, for both Hercules and Pisces a mean value of $\Delta(\log D) = -0.07$ (with D in units of $0\rlap{.}'1$) was found, while for Coma a mean value $\Delta(\log D) = -0.01$ was obtained. On the other hand, some correlation was seen between $\Delta(\log D)$ and *blue* galaxy surface brightness, such that lower surface brightness objects had larger diameter errors. This finding provided the key basis for the adopted diameter correction procedure described below.

Unfortunately, the sample of galaxies having surface photometry overlaps only partially with the cluster sample in this paper. This allows us to obtain corrected diameters directly for about only half of the galaxies in Table 2, and typically for about half of the spirals in each of our clusters. Corrected diameters for the remaining galaxies were derived as follows: For each cluster an individual [$\Delta(\log D)$, Σ_B] relation was constructed, where now $\Sigma_B \equiv B_{25} + 5 \log D(0)$, B_{25} being the blue magnitude within the circular area whose diameter is the 25th mag isophote determined by GASP, and $\log D(0)$ being the "raw" transformed UGC diameter (i.e., uncorrected for inclination or absorption effects). Examples of the relation between $\Delta(\log D)$ and Σ_B for two of our clusters is shown in Figure 2. Once B_{25} had been determined, $\Delta(\log D)$ could be obtained from a mean fit to diagrams like those in Figure 2. To estimate B_{25}, we applied a zero-point shift to the magnitude in the Zwicky *et al.* (1961–1968) catalog or in the UGC (where Zwicky magnitudes are listed for $B \leq 15.7$ mag). The zero-point shift was individually determined for each cluster by calculating the mean difference between either Zwicky or UGC magnitudes and B_{25} for those cluster galaxies having GASP photometry available. In all cases the shift ranged between -0.2 and $+0.2$ mag (with a typical dispersion of ± 0.4 mag in a given cluster).

For A2634/66, a GASP diameter was available for just one

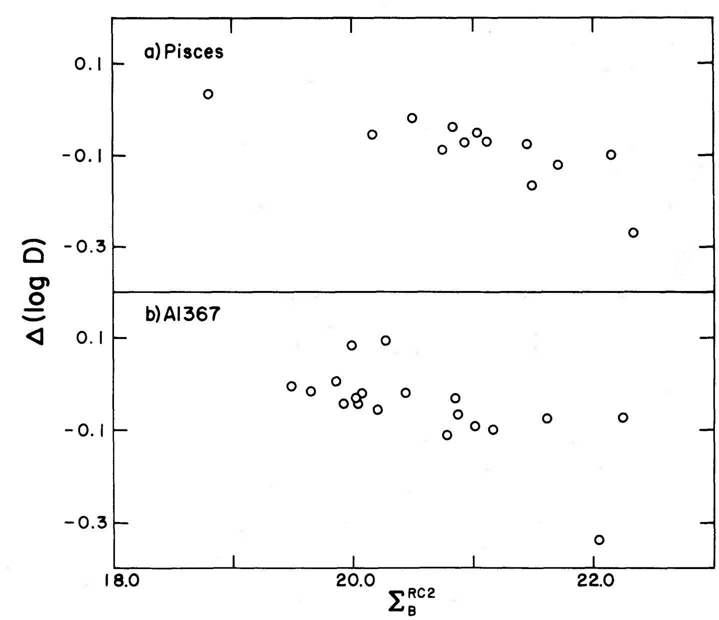

FIG. 2.—Difference between old and revised diameter values $\Delta(\log D)$ plotted against *blue* surface brightness Σ_B for objects having CCD imaging in two of our clusters. As discussed in the text, similar plots for each cluster were used to correct the diameters for those galaxies without CCD data. (Here Σ_B is determined using the old diameters, since the trend with surface brightness disappears when the new diameters are employed.)

member spiral, and for this cluster only it was necessary to use the [$\Delta(\log D)$, Σ_B] relation constructed for the entire sample, and to assume $B_{25} = B_{\rm Zwicky}$ (a result correct to within 0.1 mag for our entire GASP sample in the mean). While it would obviously be desirable to have all the cluster diameters directly measured, we believe that the above procedures yield quite satisfactory results. In particular, the slope of the [$\Delta(\log D)$, Σ_B] relation seemed more or less constant and well determined from cluster to cluster (e.g., Fig. 2), with the variation being present primarily in zero point. Furthermore, the slope of the relation is quite shallow, so that even an error of 0.5 mag in the B_{25} value translates into a typical change of only 0.03 dex in $\Delta(\log D)$. Further details of these procedures can be found in Cornell *et al.* (1985).

With the full complement of new diameters in hand, values for $H^c_{-0.5}$ and Σ_H were recalculated for the entire data set. The revised magnitudes, diameters, and surface brightnesses are given in columns (8)–(10) of Table 2, where we have distinguished estimated from actually measured isophotal diameters by listing the former in parentheses. Only these revised quantities will be used in the remaining part of the paper. Since the slope of the H-magnitude growth curve for an Sc galaxy is ~ 2.5 at $\log (A/D_1) = -0.5$ (see Paper I), for a typical $\Delta(\log D)$ value of -0.05 (i.e., 12%), we might expect the H-magnitude in the mean to become fainter by ~ 0.12 mag, and the surface brightness Σ_H to increase by $\Delta H + 5\Delta(\log D) \sim 2.5\Delta(\log D) \sim 0.12$ mag also. In point of fact, in going from the old to the new diameters, the typical change in H is usually less than that in Σ_H, owing to our having sampled the growth curve in general at values of $\log (A/D_1) > -0.5$, where the slope is shallower than the fiducial value 2.5.

Using the revised measures, a new set of mean surface brightness residuals were calculated. These values are also listed in Table 3, and are plotted against redshift in Figure 1*b*. We see there that while the trend with cluster redshift has been diminished by about one-half, a correlation remains. Hence, it appears that diameter errors only partially account for the variation in mean cluster surface brightness properties, and we must seek elsewhere for a full explanation of the effect.

One possibility is that the H band photometry itself is at fault. However, we can find no evidence for photometric errors anywhere near the size required. Further support for this claim, as pointed out by Kraan-Korteweg (1983), may come from the optical and near-red photometry of Visvanathan (1983). He observed many of the same galaxies in Cancer, Pegasus, and Z74-23 as were measured in Paper III, and found no difference in the resulting *relative* distances. A second, albeit totally ad hoc, possibility is that the intrinsic properties of the galaxies really vary from region to region in such a way as to produce by chance the effect in Figure 1*b*. A final explanation we consider involves the presence of a real selection effect. In particular, if at fixed line width, lower surface brightness objects have a greater H I content than higher surface brightness ones, the trend in Figure 1*b* might be produced, because at greater distances objects with reduced Σ will then be easier to detect at Arecibo than those with enhanced Σ. In fact, both the full cluster sample of Bothun *et al.* (1985*a*) and the isolated galaxy sample of Haynes and Giovanelli (1984; e.g., their Fig. 11) exhibit a strong relationship between hydrogen mass–to–blue light ratio $\log (M_{\rm H}/L_B)$ and surface brightness. We tentatively attribute the trend in Figure 1*b* to this type of behavior, but the problem clearly requires further study. [We note that, as shown in Figure 1, the $(1 + z)^4$ expansion effect on surface brightness only worsens the situation.]

We postpone to the next section discussion of whether the problem at hand adversely biases our distance estimates (we believe not), but it is worth noting here that in some respects the effect in Figure 1*b* is not all that large. We first illustrate this point in Figure 3, which shows the (Σ, ΔV) relations for the Virgo, Ursa Major, and distant cluster galaxies, along with the mean fit from equation (1) to the full 308-member nearby sample. There is little apparent difference in the various correlations, and, indeed, a mean least-squares fit to the 148 distant cluster objects gives

$$\Sigma_H = 17.84(\pm 0.82) - 6.93(\pm 0.33)[\log \Delta(V) - 2.5] , \quad (2)$$

in close agreement with equation (1). It is also interesting that in the four systems with the largest deviations in Figure 1*b* (A400, A539, Coma, and Hercules), the galaxies with line widths in excess of 500 km s^{-1} tend to have the largest residuals (and, if we were arbitrarily to throw out these one or two galaxies in each of the four aforementioned clusters, their residuals would drop by nearly half).

On the other hand, it is apparent that the (H, Σ_H) relation can be used for deriving distances only with very great caution, if at all. In particular, the slope of the (H, Σ_H) relation is near 2, so that any difference in Σ_H results in twice the change in

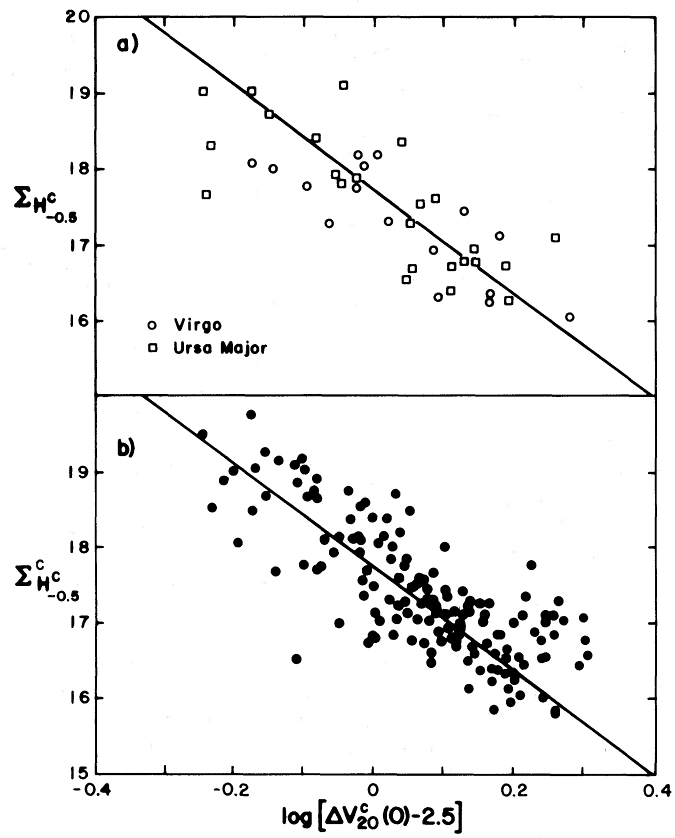

FIG. 3.—(*a*) Surface brightness/velocity-width relation for galaxies in the Virgo and Ursa Major clusters. (*b*) Same as (*a*), but for the 148 galaxies in our 10-cluster sample. The blue diameters employed are the "revised" values discussed extensively in the text. The solid line in both panels is a mean least-squares fit to 308 nearby galaxies in the Local Supercluster from Aaronson *et al.* (1982*b*).

modulus, whereas H is entered with unit slope in the IR/H I relation. Similarly, the (H, Σ_H) method is also roughly twice as sensitive to diameter errors as the IR/H I method.

As discussed earlier, the UGC transformation relations in the RC2 were derived for much larger galaxies, and so it is not surprising to find them invalid for our small-cluster objects. It may be illuminating, then, to examine why the several tests executed in Paper III led us erroneously to assume that the UGC conversion relations could be reliably applied.

One test performed in Paper III (see Fig. 5 there) involved comparison of UGC sizes with those measured using a PDS microdensitometer, in order to check for nonlinearity in the eye measurements. No such effect was found, consistent with the results here that $\Delta(\log D)$ does not correlate significantly with galaxy size. However, this test is insensitive to whether such diameters are truly isophotal. [By a curious coincidence, the Zwicky *et al.* field chosen for this test, No. 158, lies near Coma and A1367, the two clusters for which the smallest mean $\Delta(\log D)$ values were obtained!]

As a further check, transformed UGC diameters were compared in Paper III with isophotal diameters on the B_3 system of Peterson, Strom, and Strom (1979) for four galaxies each in both the Cancer and Hercules clusters. No significant differences were found. However, the comparison was made using diameters estimated from a single scan made along the major axis, and there may be a real difference between such diameters and those measured from averaged ellipticity contours, in the sense that the latter lead to results smaller by $\sim$0.03 dex in log D (see Table 10 in Paper III). Furthermore, we now have CCD data available for four of the eight tested galaxies, and the resulting GASP diameters are in the mean significantly smaller than any of the diameters for these objects listed in Paper III. We thus conclude that the sample tested there was simply too small and of too poor quality to reveal the systematic problems encountered in the present work.

An obvious concern now is how close the diameters in the RC2 are to true isophotal ones, particularly for those galaxies used to calibrate the zero point of the IR/H I relation, and for those in the Virgo Cluster used below to constrain Virgocentric motion. Fortunately, there are several reasons for having some confidence in these diameters. First, many of our Virgo objects, along with M31 and M33, are among the primary photometric standards listed in the RC2. Second, a comparison of *ellipticity-fit* diameters of 18 Virgo cluster spirals from Peterson, Strom, and Strom (1979) with the corresponding RC2 diameters yielded $\Delta(\log D) = -0.01 \pm 0.01$ (see Table 10 of Paper III). Finally, while the CCD field of view on the No. 1 0.9 m telescope was generally too small to contain the full extent of most Virgo galaxies of interest, for the one object we did manage to observe (NGC 4651), a value $\Delta(\log D) = +0.01$ was derived. Clearly, accurate surface photometry of nearby galaxies is of considerable importance for the distance-scale problem. A program to obtain such photometry has recently been initiated by Pierce and Tully (1984), and we await with interest the fruition of this work.

V. DISTANCE MODULI AND HUBBLE RATIOS TO 10 GALAXY CLUSTERS

a) Possible Sample Bias

In Figure 4 we present the IR/H I diagrams for our 10 galaxy clusters. Reasonably well-defined relations are apparent in all 10 cases. Before deriving distances, however, we need to address a number of potential problems which could lead to bias in the results. These include curvature in the relation, Malmquist error, H I signal-to-noise and flux effects, and the surface brightness differences already discussed. We will find that only the first of these problems requires explicit attention.

TABLE 4

SLOPE OF THE LINEAR IR/H I RELATION IN 12 CLUSTERS

Cluster	$-b$	σ	$\|r\|$	N
Pisces	10.83	0.42	0.97	20
A400	8.26	1.12	0.92	7
A539	9.62	1.47	0.87	9
Cancer	10.73	0.98	0.87	22
A1367	11.53	1.11	0.87	20
Coma	9.86	0.76	0.94	13
Z74-23	13.78	1.17	0.93	13
Hercules	7.84	1.18	0.85	11
Pegasus	9.99	0.80	0.89	22
A2634/66	7.73	1.03	0.87	11
Virgo	10.29	0.68	0.94	16
Ursa Major	10.53	0.43	0.97	24
Mean[a]	10.34	...	...	...

[a] Weighted by galaxy number in each cluster.

i) *Curvature Effect*

The IR/H I relation is nonlinear, an effect easily visible, for instance, in Figure 2 of Aaronson *et al.* (1982*b*). Because of the restricted sample size, the curvature is less obvious for the data in Figure 4 here, but its presence is clearly indicated by the results in Table 4. There we list the slopes obtained by applying linear least-squares fits to the individual cluster relations. The mean slopes range from a low of 7.7 for A2634/66 to a high of 13.8 for Z74-73, but generally fall near and have an average close to the fiducial value of 10.[3] However, there is a clear trend with cluster redshift, such that the more distant systems tend to have shallower slopes. This is precisely the effect expected from a curved relation, because, as we advance in redshift, the brighter, right-hand side of the IR/H I diagram (i.e., the side having log $\Delta V > 2.5$) becomes increasingly more populated relative to the fainter, left-hand side (see Fig. 4).

In the past, we have always employed a linear IR/H I relation. This has led to acceptable results because in our earlier work we have generally evenly populated the IR/H I plane, so that the effect of residual curvature was more or less canceled out. It is clearly necessary here, however, to explicitly account for the effect so that a distance bias is not introduced.

We have two choices at this point. The curvature is no doubt due partially to the increasing influence of nonrotational support in galaxies of smaller mass. We might apply, then, a velocity dispersion correction following, for instance, the scheme of Bottinelli *et al.* (1983). Unfortunately, the amount of noncircular motion required to fully "straighten out" the IR/H I relation seems larger than actual dispersion measurements indicate (e.g., Lewis 1984; Richter and Huchtmeier 1984;

[3] We note that the mean slope in the *blue* luminosity/line width relation obtained from our cluster data is -6.5. This value is intermediate between the slopes of -5 and -7.2 found in the recent work of Bottinelli *et al.* (1983) and Richter and Huchtmeier (1984), respectively. It is considerably less, however, than the slopes of -10 to -13 obtained in several studies by Rubin and collaborators (Rubin, Burstein, and Thonnard 1980; Rubin *et al.* 1982).

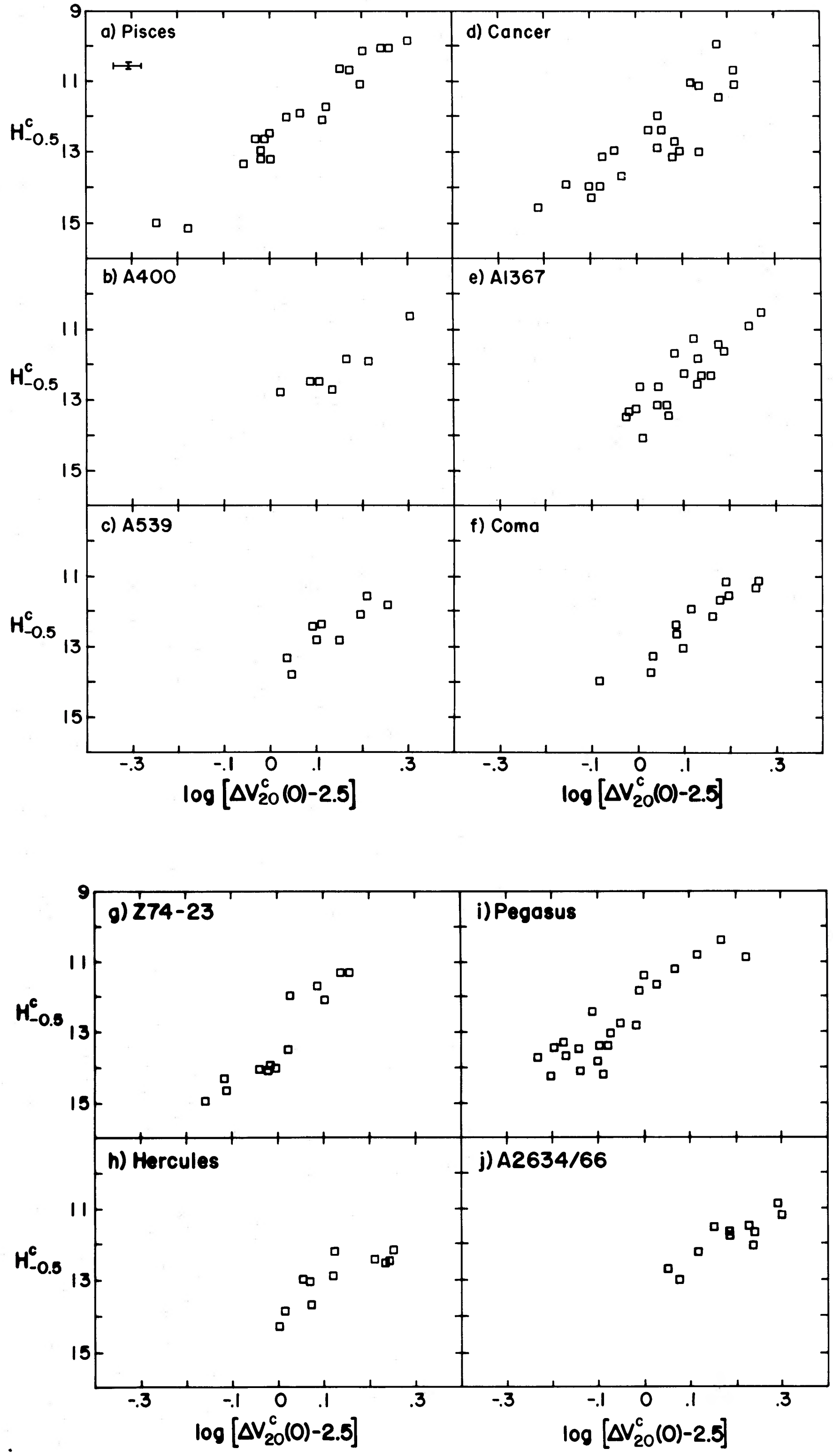

FIG. 4.—(*a–j*) Infrared magnitude/H I velocity-width relation for the 10 galaxy clusters in our sample

Tully and Fouqué 1985; Skillman 1985). Furthermore, Bothun *et al.* (1984*b*) have suggested that a dependence of metallicity on disk luminosity can also contribute to curvature in the relation. Hence, it does not seem to us that a dispersion correction can be unambiguously applied.

Alternatively, we take a strictly empirical viewpoint and choose to adopt a quadratic form of the IR/H I relation, that is, a form given by

$$H^{\rm abs} = a + b(\log \Delta V - 2.5) + c(\log \Delta V - 2.5)^2 \; . \qquad (3)$$

Such an expression has already been investigated for the 300 galaxy Local Supercluster sample by AHMST. We shall adopt directly from their Table 3 the coefficients $b = -11.18$ and $c = 7.5$, values which take explicit account of the Virgocentric velocity field.

In Figure 5 we compare the quadratic IR/H I relation with the linear relation of slope 10 used in our previous efforts. It can be seen that the two calibrations are closely similar over most of the range of interest, diverging significantly only at the high and low velocity width ends. We stress that outside the velocity-width limits shown in Figure 5, the IR/H I relation remains ill defined and should be applied only with very great caution.

The moduli obtained using equation (3) are typically larger by $\lesssim 0.1$ mag than those derived with our former relation. For a sample that evenly populates the IR/H I plane, this difference is a reflection primarily of the steeper slope in the linear term (-11.18 versus -10), rather than the presence of the quadratic term per se. This point was discussed in both Paper I and Paper IV, where it was noted that ignorance of the exact slope in the IR/H I relation leads to a small, ~ 0.1 mag uncertainty in modulus. A similar result was found by Sandage and Tammann (1984*b*) in their reanalysis of our earlier data. Although these authors consider the effect important, this 0.1 mag ambiguity is rather negligible in comparison with the *very much greater* uncertainty in distances to the nearby calibrating galaxies, a point discussed further below.

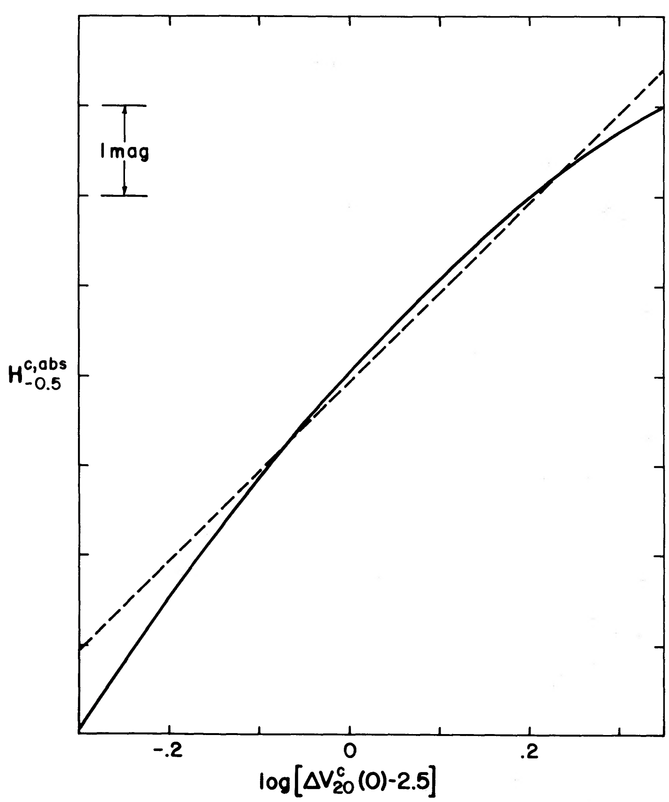

FIG. 5.—A comparison of the quadratic and linear forms of the IR/H I relation. The relative zero points were determined using the three calibrating galaxies in Fig. 7. The two curves differ significantly only at very small and very large velocity widths, where coincidentally the empirical form of the relation remains ill defined.

Richter and Huchtmeier (1984) have recently explored interplay between the slope, zero-point, and derived moduli using a *blue* luminosity/line-width relation. Curiously, these authors find a much larger dependence of final distance on slope (their Table 6) than is obtained either by us or by Sandage and Tammann (1984*b*) in the infrared. The reasons for this are not entirely clear to us, but it may involve the fact that Richter and Huchtmeier's Local Group calibrating galaxies are dominated by low-luminosity, small line width objects, while their more distant groups are more weighted by higher luminosity, large line width systems. In particular, the interplay between slope and zero point is determined by the degree to which the calibrating galaxies are uniformly distributed in the IR/H I plane, and the net effect on distances will depend on this as well as on the similarity in loci between the object and calibrating galaxies. In order to minimize the slope dependence (and for that matter, to control any hidden systematic errors), it is clearly desirable to populate the IR/H I diagram in as uniform a fashion as possible.

ii) *Magnitude Selection*

A second potential bias to consider is the familiar Malmquist effect, which has undoubtedly plagued much past distance work. Fortunately, with clusters we confine ourselves to a sample which is basically volume- rather than magnitude-limited, allowing us to circumvent the problem. To test explicitly for Malmquist selection, we have in each of our cluster samples searched for a relation between velocity and velocity width (cf. Paper III; Roberts 1978). In no case was a significant trend found.

There is another magnitude selection effect that we should consider. Since the width of the IR/H I relationship is finite, our moduli could still be biased, because in any given cluster we take a horizontal (or magnitude) cut through the data rather than a perpendicular one. The amount of prejudice introduced by this effect is related to both the scatter of the IR/H I relation (which is small) and the depth in magnitude to which the relation is sampled. We can see in Figure 4 that the sampling is sufficiently deep in all of our clusters to yield a clear relationship, minimizing the possible bias. Furthermore, over the sampling depth in each cluster our standard candles are H I– and not magnitude-selected. We believe that this consideration eliminates any need for the sort of correction being discussed.

Our contention that magnitude-selection problems can be ignored with the present sample is supported by the results obtained in § VII, where (after correcting for the appropriate Local Group motion) we find no significant correlation between cluster redshift and Hubble ratio. Indeed, our four lowest redshift clusters (Pegasus, Cancer, Pisces, and Z74-23) are sampled as deep in magnitude and velocity width as the

Virgo fiducial, yet show little mean difference in Hubble ratio from the remaining, less well-sampled systems.[4]

iii) H I *Signal-to-Noise Ratio*

The next problem to address concerns the fact that the signal-to-noise (S/N) ratios of our H I profiles generally decrease with increasing redshift. If our derived velocity widths are sensitive to S/N ratio in a systematic fashion, the resulting distances would also be so biased.

Fortunately, the effect of noise on H I profiles has been extensively investigated by Lewis (1983) via Monte Carlo simulations. The basic results for maximizing and minimizing algorithms (i.e., those which determine the line width by working from the outside in or from the inside out) are summarized in his Tables 2 and 3. These results clearly show that, in contrast to maximizing procedures, minimizing ones are very insensitive to degradation of the H I profile. For instance, starting with a fiducial profile having an S/N ratio of 57 (using the Lewis convention), the 20% line width ΔV_{20} was found to decrease by only $\sim$0.4% down to a level of S/N $\sim$ 7. Curiously, ΔV_{20} appeared slightly more stable against noise in the minimizing tests than either ΔV_{50} or ΔV_{75}. In any event, since S/N $\sim$ 7 for Lewis (1983) corresponds roughly with the cutoff S/N level used here, and because, further, our velocity width is defined at the 20% level via a minimizing algorithm, we conclude that S/N bias is unlikely to be present in our data set.

iv) H I *Flux*

To test whether the increasingly more severe H I flux limit could cause a bias with distance, we tested an additional term in equation (3). This correction was proportional to the H I flux excess relative to a Virgo/Ursa Major galaxy of the same velocity width. In 200 galaxies with known distances relative to Virgo (Aaronson *et al.* 1982*b*), we found no significant dependence on H I flux as a second parameter. Significant bias in distance from this cause can be ruled out.

We emphasize that this test is distinct from the one performed by AHMST. Aside from a quadratic form these authors considered a number of possible *second-order* corrections to the IR/H I relation, including surface brightness, morphological type, and H I flux. However, all of these "improvements" are in fact highly correlated. In the test employed here, we have considered whether the H I flux can be used as a *third-order* correction, after allowing for the more dominant second-order effect via the quadratic velocity-width term.

v) *Surface Brightness*

While the surface brightness effect in Figure 1 results in an underestimate of distance with the (H, Σ_H) method, there is no *a priori* sense in which distance from the IR/H I method is biased, because any linear combination of magnitude and diameter changes can alter Σ. However, it is possible to test empirically whether and how a differing surface brightness leads to an altered location in the IR/H I diagram by examining correlations of residuals within the clusters themselves. That is, for every galaxy we can determine the residual in H-magnitude from the best fit of equation (3) to each cluster and compare this with the corresponding surface brightness residual. The result of applying this test to our 10-cluster sample is shown in Figure 6.

The residuals weakly correlate, and a least-squares fit to the data in Figure 6 yields a slope of 0.3. The trend is such that at fixed velocity width, lower surface brightness galaxies tend to fall *below* the mean fit IR/H I relation. We could now in prin-

[4] We make passing note of two recent studies by Teerikorpi (1984) and Bottinelli *et al.* (1985) discussing the Malmquist effect and the luminosity/line width relation. We certainly agree with those authors that for magnitude-limited samples of field galaxies the problem needs to be dealt with. We are puzzled, however, by Bottinelli *et al.*'s discussion of the paper by Bothun *et al.* (1984*a*), where we attempt to apply the IR/H I method to a sample of field Sc I spirals. Bottinelli *et al.* imply that because the corrected Bothun *et al.* data still exhibited a correlation between Hubble ratio and distance (though we are not able to reproduce as steep a dependence as they show), our adjustment for Malmquist effect was too small, and the derived H_0 value too large. In fact, since the correction we used is equivalent to a simple zero-point shift, it will not alter any Hubble ratio–distance trend. The same comment may apply to the similar claim by Sandage and Tammann (1984*c*, 1985) that the Bothun *et al.* results are undercorrected for Malmquist bias, although we are unsure of this, since the reference they cite is not yet available. In any event, we emphasize that the primary purpose of the Bothun *et al.* study was to demonstrate the lack of environmental influence on the IR/H I relation. We note that it is likely, however, that the isophotal diameter problems discussed in this paper also affect the Bothun *et al.* results.

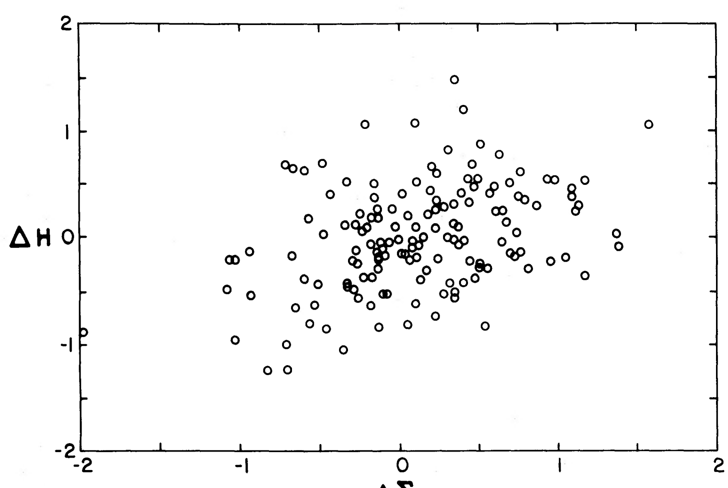

FIG. 6.—A plot of the H-magnitude residual ΔH about the mean quadratic IR/H I relation against surface brightness residual $\Delta\Sigma_H$ ($=\Sigma^{\rm obs} - \Sigma^{\rm pred}$; cf. Fig. 1) for the 10-cluster sample. Both quantities are determined at fixed velocity width. The sense of the weak trend is such that galaxies *at constant width* having lower surface brightness are underluminous at H. Hence, any bias introduced into the IR/H I relation by the trend in Fig. 1 is likely to be toward larger distances.

ciple correct for the bias in Figure 1 by including an additional expression in equation (3) of the form $0.3(\Sigma^{obs} - \Sigma^{pred})$. The net effect of such a term (which we again emphasize is distinct from the AHMST correction) would be to *decrease* the moduli of our more distant clusters by ~ 0.1 mag. We have chosen to forgo this potential improvement because we consider the effect only marginally established (the correlation coefficient in Fig. 6 is just 0.38). Again, we will ultimately find little difference in mean Hubble ratio for clusters having small and large values of $\langle \Sigma^{obs} - \Sigma^{pred} \rangle$. We emphasize, however, that the trend in Figure 1 appears such as to bias our results toward *lower* values of H_0.

b) Absolute Calibration

We seek now to find a value of the constant a in the expression

$$H^{c,abs}_{-0.5} = a - 11.18[\log \Delta V^c_{20}(0) - 2.5] + 7.5[\log \Delta V^c_{20}(0) - 2.5]^2 . \quad (4)$$

A number of important developments have occurred since our discussion of this topic in Paper IV, although the overall situation remains probably as confused and controversial as ever. Perhaps the most significant new result comes from Freedman's (1985) *BVRI* Cepheid observations in M33, which yield a preliminary true modulus of ~ 24.1 mag. These observations seem to demonstrate both the presence of internal reddening and the existence of scale errors in the older photographic photometry of Hubble and Sandage. Sandage and Carlson's (1983) proposed increase in the M33 modulus to 25.35 mag and the implications which follow therefrom must now be largely discounted. Freedman's data show that the M33 Cepheids are on average internally extincted by $A_V \sim 0.6$ mag, and it seems clear that future Cepheid and brightest supergiant observations must pay careful attention to such absorption effects.

For the present purpose, we shall derive a calibration based on recent H band and CCD observations of Cepheids to three galaxies—M31, M33, and NGC 2403. We regard these results, though still in a preparatory stage, as having greater reliability than other methods. In particular, as discussed by McGonegal *et al.* (1982), IR photometry minimizes extinction, metallicity, and variability effects. However, even for comparatively nearby galaxies such as M31, these advantages are perhaps offset by crowding problems and lack of detector sensitivity. Currently, the I band CCD observations probably yield the most trustworthy moduli. Nevertheless, metallicity dependence in the Cepheid *P-L* relation from intrinsic (i.e., stellar interiors) causes remains a source of concern.

The zero-point derivation is summarized in Table 5 and Figure 7. For M31 we adopt a modulus of 24.12 mag from Welch *et al*'s (1985) H band Cepheid observations in Baade's fields I–III, with an infrared *P-L* relation calibrated from Caldwell (1983). For M33, McAlary and Welch (1985) report a modulus of 24.17 mag, again using the Caldwell calibration. With the identical data, but using an IR *P-L* relation determined instead with, in our opinion, a less reliable calibration from Fernie and McGonegal (1983), Madore *et al.* (1985) obtain an M33 modulus of 24.3 mag. Combining these results with Freedman's (1985) M33 modulus of 24.1 mag leads us to adopt an M33 modulus of 24.17 mag.

We note that with the Caldwell (1983) scale the IR Cepheid photometry leads to a Large Magellanic Cloud modulus of 18.5 mag (see McAlary and Welch 1985), which is the same distance assumed by Freedman (1985) in her work. Such a result is identical with the LMC modulus recently advocated by Feast (1985). The Feast number is itself based on the average of a variety of methods (which do not, however, include the IR Cepheid measurements), into which endemic problems with galactic open cluster main-sequence fitting (and in particular the Hyades modulus) enter with very little weight.

Finally, for NGC 2403 we adopt a modulus of 27.5 mag, a result which comes from new CCD observations of Madore and Freedman (1985) for a dozen Cepheids. While this distance is close to the original Tammann and Sandage (1968) value, it is substantially less than that found from the J (1.2 μm) band Cepheid observations summarized by McAlary and Welch (1985). However, both Madore (1985) and the present authors regard the latter result, based on generally poor-quality observations of only five stars, with very low weight, owing to the

TABLE 5

PRELIMINARY ZERO-POINT CALIBRATION OF THE QUADRATIC IR/H I RELATION

Galaxy	$m - M$ (mag)	$H^{c,abs}_{-0.5}$ (mag)	a (mag)
M31	24.12[a]	−23.21	−20.92
M33	24.17[b]	−19.79	−20.94
N2403	27.5[c]	−21.05	−21.29
Mean	...	...	-21.05 ± 0.12

[a] Adopted from Welch *et al.* 1985.
[b] Adopted from McAlary and Welch 1985; Freedman 1985; and Madore *et al.* 1985.
[c] Adopted from Madore and Freedman 1985.

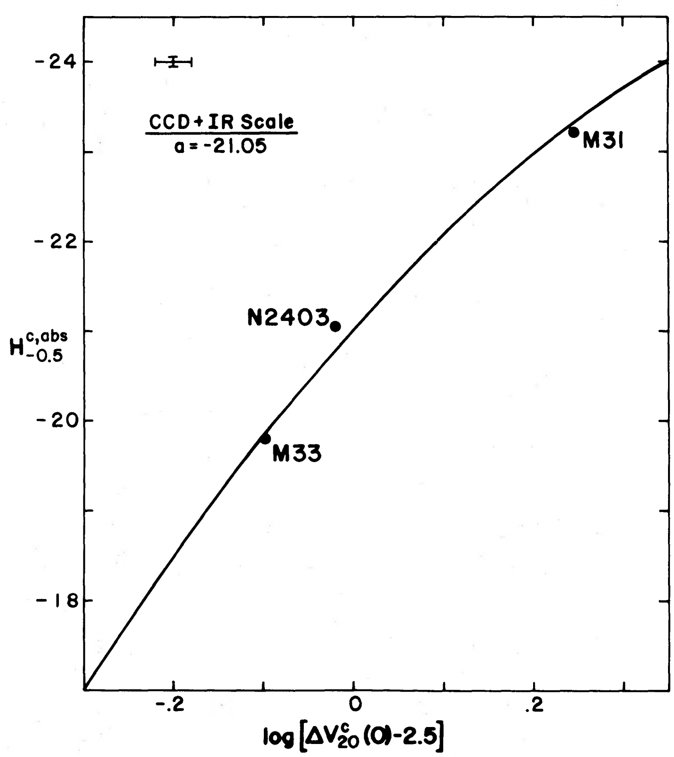

FIG. 7.—Adopted absolute calibration of the quadratic IR/H I relation based on modern infrared and CCD measurements of Cepheids.

difficulties with photometry in distant systems alluded to earlier. With our three adopted distances, a zero point of $a = -21.05$ mag directly follows.[5]

Two alternative zero-point calibrations are shown in Figure 8. These are based on the (older) Sandage-Tammann local scale (Fig. 8*a*) and the de Vaucouleurs local scale (Fig. 8*b*) (see § IV*a* of Paper IV for an explicit listing of the specific distances). We refer to Figure 8*a* as the "older" Sandage-Tammann scale because it does not include the aforementioned larger—but probably incorrect—M33 modulus of Sandage and Carlson (1983), or the larger M81 modulus used by Sandage and Tammann (1984*b*). Note that our adopted zero point in Figure 7 falls intermediate between the two in Figure 8 (which differ from each other by 0.65 mag), but closer to the de Vaucouleurs scale.

It should be clear that the situation with regard to local distances is by no means closed. For instance, while we regard the Figure 7 zero point with higher weight than either of those in Figure 8, the considerable scatter seen in the infrared *P-L* relations for M31 and M33, a result almost certainly of crowding problems, is nonetheless disturbing. Even so, the excellent agreement between the IR and CCD distances to the M33 Cepheids suggests that there are no hidden systematic errors in at least the M33 infrared photometry.

[5] Sandage and Humphreys (1980) have called into question the use of M33 as a suitable IR/H I calibrator, owing to their claim of the presence of a severe inner warp in the disk. However, in Paper IV we have argued against the reality of such a warp because of the lack of any apparent distortion in available high-resolution H I maps. Recently, Maucherat *et al.* (1984) performed careful optical surface photometry on M33 and have concluded that there is indeed no severe inner warping. In particular, they find the zero-age population component to be perfectly fitted by a logarithmic spiral. They also find that the wider, older part of the stellar arms are systematically displaced outward from the zero-age component (but lie nevertheless in the same plane), an effect which apparently led Sandage and Humphreys to propose the spurious inner warp. Hence, there seems to be little reason now to doubt the validity of M33 as a calibration galaxy.

There are, however, other indications which suggest that our adopted zero point might still be readily pushed in *either* direction. For example, there is at present an outstanding discrepancy between the distances to galactic clusters containing Cepheids obtained from main-sequence fitting and those derived from Hβ photometry (e.g., Schmidt 1984; further confirmed by Balona and Shobbrook 1984), in the sense that the latter gives smaller distances by ~ 0.3 mag. Curiously, the resulting differences on the *extragalactic* Cepheid scale are not so large when broad-band optical observations are employed (e.g., Feast 1985), but they become substantial when applied to calibration of the infrared *P-L* relation. For instance, Schmidt's (1984) Hβ measurements lead to an LMC modulus of 18.51 mag using the optical data, but only 18.17 mag with the IR photometry (versus the earlier-quoted 18.5 mag from the Caldwell main-sequence distances). This latter result is, interestingly enough, in excellent concurrence with the LMC modulus of 18.2 mag obtained by Schommer, Olszewski, and Aaronson (1984) from main-sequence fitting. A short (< 18.5 mag) modulus is further supported by new LMC work on RR Lyrae stars by Walker (1985) and on Mira variables by Menzies and Whitelock (1985). Additional evidence for a shrunken *galactic* scale via a decrease in galactic center distance comes from recent studies of globular cluster kinematics (Frenk and White 1982) and RR Lyrae stars (Blanco and Blanco 1985). The moral here seems to be that major problems exist with the galactic Cepheid scale which require sorting out.

On the other hand, in contrast to the above results, which generally imply an even more contracted universe, there are the new distances to M31 and M33 obtained by Mould and Kristian (1985) using the luminosity of the first giant-branch tip in the halo components of these galaxies. These authors find moduli of 24.4 ± 0.2 for M31 and 24.8 ± 0.2 for M33, values which are in almost precise agreement with those on the (older) Sandage-Tammann scale used in the construction of Figure 8*a*! We also note the recent nova modulus to M31 of 24.35 ± 0.2 mag found by Cohen (1985) from an improved

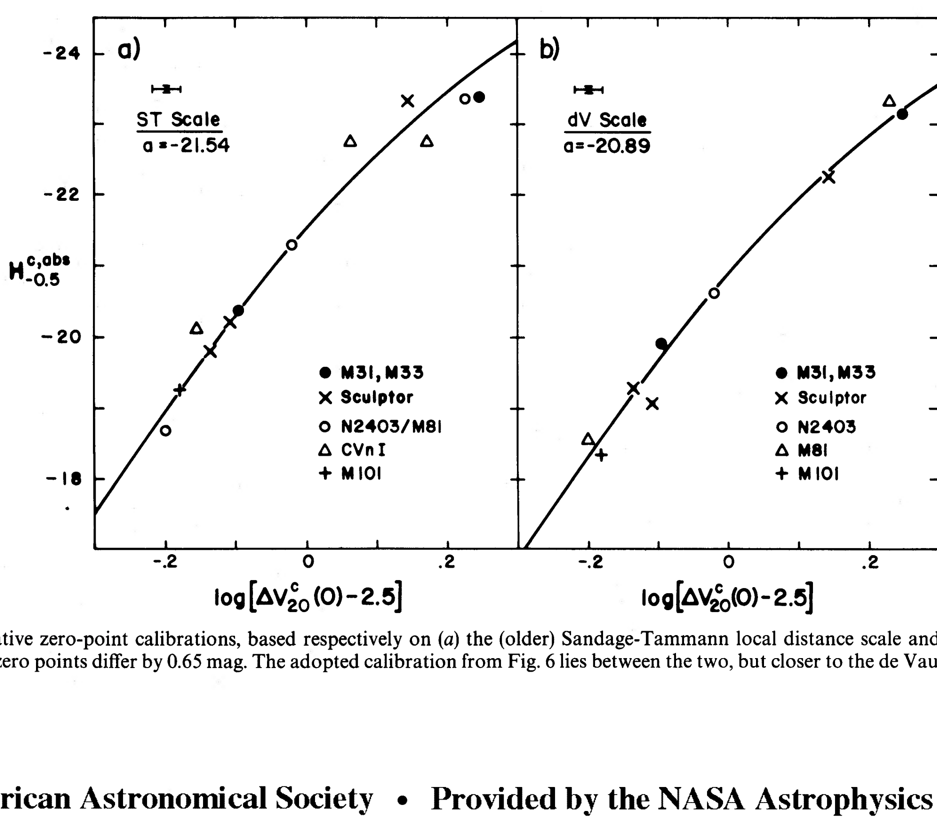

FIG. 8.—Two alternative zero-point calibrations, based respectively on (*a*) the (older) Sandage-Tammann local distance scale and (*b*) the de Vaucouleurs local distance scale. The two zero points differ by 0.65 mag. The adopted calibration from Fig. 6 lies between the two, but closer to the de Vaucouleurs scale.

TABLE 6

MEAN DISTANCE MODULI AND HUBBLE RATIOS

Cluster (1)	$\langle m-M \rangle$ (mag) (2)	σ (mag) (3)	$\Delta(m-M)$ Virgo (mag) (4)	$\langle r \rangle$ (Mpc) (5)	$\langle V \rangle / \langle r \rangle$ (km s^{-1} Mpc^{-1}) (6)	$\langle V/r \rangle$ (km s^{-1} Mpc^{-1}) (7)	Mean H_0[a] (km s^{-1} Mpc^{-1}) (8)	Mean V[b] (km s^{-1}) (9)	MWB ΔV[c] (km s^{-1}) (10)	Corrected H_0 (km s^{-1} (Mpc^{-1}) (11)
Pisces	33.59(0.09)	0.39	2.77(0.15)	52(2)	101(4)	103(4)	102(3)	5323(58)	−490	92(3)
A400	34.55(0.14)	0.36	3.73(0.18)	81(5)	88(6)	98(7)	93(4)	7559(90)	−243	90(4)
A539	34.89(0.12)	0.35	4.07(0.17)	95(5)	90(5)	91(6)	91(4)	8622(123)	72	92(4)
Cancer	33.82(0.15)	0.71	3.00(0.19)	58(4)	82(6)	83(4)	83(4)	4809(89)	325	88(4)
A1367	34.35(0.11)	0.49	3.53(0.16)	74(4)	87(4)	90(5)	88(3)	6538(73)	392	94(4)
Coma	34.51(0.10)	0.34	3.69(0.16)	80(4)	87(4)	92(4)	90(3)	7158(45)	255	93(3)
Z74-23	34.25(0.15)	0.55	3.43(0.19)	71(5)	85(6)	84(5)	85(4)	5996(153)	280	89(4)
Hercules	35.25(0.13)	0.43	4.43(0.18)	112(7)	99(6)	97(5)	98(4)	10962(97)	−20	98(4)
Pegasus	32.97(0.14)	0.64	2.15(0.18)	39(3)	104(7)	111(6)	108(5)	4224(78)	−559	93(4)
A2634/66	34.65(0.10)	0.34	3.83(0.16)	85(4)	103(5)	102(4)	103(3)	8749(115)	−581	96(3)
Virgo	30.82(0.12)	0.49	...	14.6(0.8)	74(5)	...	...	1073(38)	290	93(6)
Mean	...	...	...	...	...	...	94(3)	...	...	92(1)

NOTE.—Numbers in parentheses are standard deviations of the mean.

[a] Mean of cols. (6) and (7).

[b] Mean of col. (5) multiplied by col. (8).

[c] Correction to col. (9) for Local Group motion toward the dipole anisotropy. The Virgo correction is for Local Group motion within the Supercluster only.

Galactic calibration. However, even a modest (and probably required) correction for internal absorption in M31 would reconcile this distance with our adopted value. Clearly, it cannot be emphasized enough that much work remains before an unassailable calibration of the IR/H I relation is at hand.

c) *Distances and Hubble Ratios*

Listed in column (11) of Table 2 are absolute H-magnitudes calculated from equation (3) above using the zero-point coefficient $a = -21.05$ mag from Table 5. Columns (12) and (13) contain the corresponding distance moduli and distances. An individual Hubble ratio for every galaxy, obtained by dividing the velocity in column (4) by the distance in column (13), is given in column (14).

The mean results for each cluster are tabulated in the first part of Table 6. Column (2) there gives the average of the moduli from column (12) in Table 2, and the 1 σ dispersion of this average is listed in column (3). The relative distance modulus of each cluster with Virgo is given in column (4). The average cluster distance $\langle r \rangle$ is in column (5), and the Hubble ratio obtained by dividing the mean cluster redshift $\langle V \rangle$ in column (6) of Table 1 by $\langle r \rangle$ is in column (6). Finally, column (7) of Table 6 gives $\langle V/r \rangle$, the mean of the individual galaxy Hubble ratios from column (14) of Table 2. The results for Virgo listed at the bottom of the table are derived from the data in Aaronson *et al.* (1982*b*). Also, the standard deviation of the mean is given in parentheses after each entry, excluding in all cases the unknown zero-point error of the calibration, and hence reflecting only the observed scatter of the data for each cluster.

The 1 σ scatter of the cluster IR/H I relations are generally seen to be in the range 0.35–0.50 mag, consistent with the canonical $\sigma \sim 0.45$ mag (Paper IV). The scatter is, however, found to be rather larger for three clusters—Cancer, Z74-23, and Pegasus. In the first two cases this increased scatter appears to be a result of true clusters not being present. The structure of Cancer has been investigated in detail by Bothun *et al.* (1983), who describe this system as "an unbound collection of groups." These authors divide Cancer up into five major subgroups which they label A–E. In Table 2 after each Cancer galaxy name we have listed in parentheses the subgroup to which the object belongs, and in Figure 9*a* we have plotted the mean of the subgroup moduli from Table 2 against the mean subgroup velocities from Table 2 of Bothun *et al.* (1983). A clear relation is present between subgroup distance and velocity, confirming the conclusions of Bothun *et al.* (1983) that Cancer consists of separate clumped structures.

A similar situation appears to hold for Z74-23. The velocity

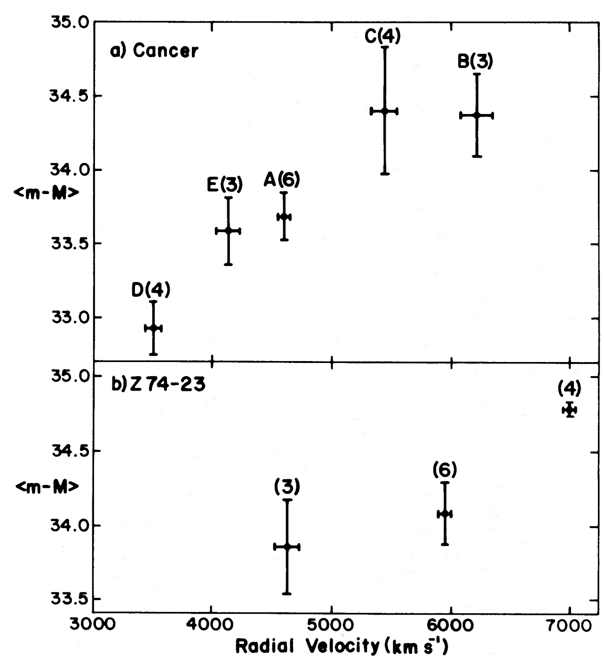

FIG. 9.—Mean distance modulus plotted against radial velocity for five subgroups in the Cancer cluster (*a*) and three subgroups in cluster Z74-23 (*b*). These diagrams confirm the impression from radial velocity studies that both "clusters" are really composed of unbounded substructures strung out in space.

histogram of this system is in fact divided into three well-defined clumps roughly centered at 4500, 6000, and 7000 km s^{-1}. In Figure 9*b* we have plotted the mean moduli from Table 2 for the galaxies in each clump against the mean clump velocity, and a significant correlation is again present.

The large scatter seen for Pegasus is unexpected. However, depth effects may once again contribute some of this scatter, since there is some correlation between distance modulus and velocity for the individual spirals. In particular, several of the higher redshift objects may belong to the background Perseus-Pisces Supercluster (e.g., Richter and Huchtmeier 1982) rather than to Pegasus I proper. Pegasus also has a large fraction of objects of small velocity width, and there is a suggestion from Figure 4*i* here and Figure 2 of Aaronson *et al.* (1982*b*) that scatter in the IR/H I diagram increases for low-mass spirals, possibly because of growing stochastic influence from non-circular motions. Indeed, a few of the low-luminosity objects in several of our clusters have Gaussian-shaped H I profiles and inclinations which may not be well determined. It may be arguable whether such systems should even be included in the sample, although their presence does not seem to introduce any clear distance bias.

In two more of our other clusters, Hercules and A2634/66, some correlation is again found between the individual moduli and radial velocities. Note that for these and the three aforementioned systems, the dispersion in $\langle V \rangle / \langle r \rangle$ is *larger* than for $\langle V/r \rangle$, which is expected to occur only if we are viewing objects that are somewhat strung out along the line of sight. On the other hand, there is no evidence of any velocity-distance trend for the individual cluster spirals in either A1367 or Coma. These two clusters are embedded in the well-known Coma Supercluster, and since many of the objects we have observed in them are outlying members, we are likely to be sampling part of the supercluster as well. Hence, the absence of any well-defined velocity-distance effect suggests that, at least at the locations of A1367 and Coma, the supercluster is thin.

The cluster distances in Table 6 are seen to range from Pegasus at ~ 40 Mpc to Hercules at ~ 110 Mpc. The Hubble ratios generally scatter from ~ 80 to 110 km s^{-1} Mpc^{-1}, with individual errors (again with zero-point uncertainty excluded) that are typically ~ 5 km s^{-1} Mpc^{-1}. In all cases the cluster Hubble ratios exceed that of Virgo at ~ 74 km s^{-1} Mpc^{-1} (see Table 6, bottom). In general, the agreement between the Hubble ratio calculated from $\langle V \rangle / \langle r \rangle$ or $\langle V/r \rangle$ is quite good, even perhaps fortuitously for Cancer and Z74-23 (cf. Fig. 9). The two largest discrepancies are for A400 and Pegasus, and in both cases this is largely a reflection of the difference between the mean cluster redshift and the mean redshift of our observed sample (see cols. [6] and [8] of Table 1).

The velocity histograms for most of our clusters are in fact rather broad. In view of this point and the ambiguities involved with depth effects discussed earlier, we shall in the discussion which follows make use solely of the Hubble ratio obtained from the average of the $\langle V \rangle / \langle r \rangle$ and $\langle V/r \rangle$ values. This mean ratio is listed in column (8) of Table 6, and the redshift corresponding to this mean and the distance from column (5) is given in column (9). The mean Hubble ratios are shown plotted against these "compromise" velocities in Figure 10*a*, which graphically illustrates the large scatter of Hubble ratios in comparison with the individual errors, a point we take up in the next section.

We note in passing that the relative Virgo-Coma distance modulus from column (4) of Table 6 is 3.69 ± 0.16 mag, in excellent agreement with the relative modulus of 3.75 ± 0.18 mag found by Dressler (1984) from the luminosity/velocity-dispersion relation for elliptical galaxies. It does not, however agree well with Dressler's alternative relative modulus of 4.00 ± 0.18 mag obtained from the luminosity/Mg index relation. While Sandage and Tammann (1984*b*) attach high weight to the *mean* of Dressler's two discrepant values, the physical basis of the luminosity/Mg index relation is not well established, and we consider its reliability as a valid distance indicator to be unproved. Other generally low-weight determinations of the relative Virgo-Coma modulus have been summarized recently by Tammann and Sandage (1985).

Finally, to assess the possible effect of not applying a cor-

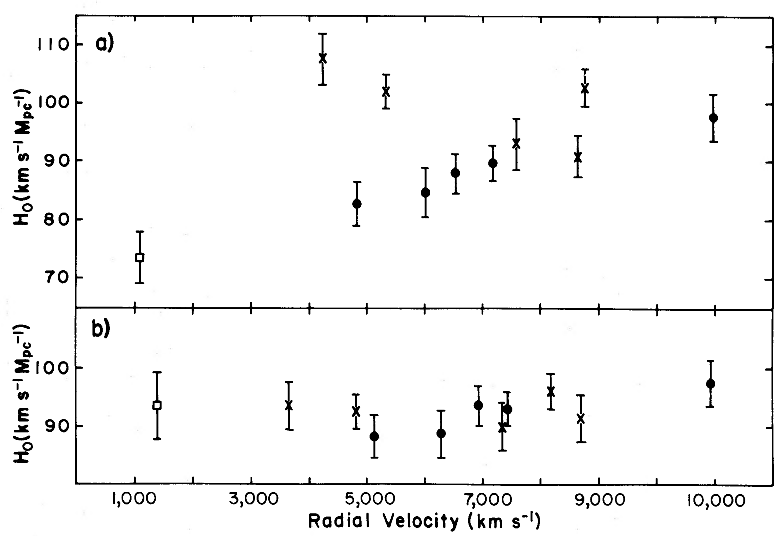

FIG. 10.—(*a*) Observed Hubble ratio plotted against radial velocity for the cluster sample. Clusters in the north Galactic cap are plotted as filled circles, clusters in the south Galactic cap are plotted as crosses, and the Virgo Cluster is plotted as an open square. Note how the scatter of the data is considerably larger than the individual errors. Formal minimization yields a velocity component in close agreement with the 3 K dipole anisotropy. (*b*) Hubble ratios after correcting the mean cluster velocities for the observed dipole anisotropy. For Virgo, a Local Group Virgocentric motion of 290 km s^{-1} was assumed.

rection for inclination i to the observed H-magnitudes, we have calculated least-squares fits of i against $m - M$ for members of each cluster. No significant correlations were found. (Similar fits of i against surface brightness, surface brightness residual, and magnitude residual [i.e., Fig. 6] were also examined, but with null results.) However, a small dependence of modulus on inclination does emerge if the sample is divided into two bins of roughly equal size, having $i \leq 70°$ and $i > 70°$. The higher inclined galaxies then give moduli that are in the mean larger by ~ 0.15 mag, presumably reflecting a small amount of internal absorption, but the difference is significant only at the 1 σ level. Both the calibrators and the cluster objects are about uniformly distributed in i, so any possible bias in this regard would be very tiny.

VI. TESTS FOR APPARENT ANISOTROPY IN THE HUBBLE FLOW

In this section we search for signals in our data that reflect deviations from uniform Hubble flow. We first show that the scatter in the Hubble ratios of our 10-cluster sample arises from a missing velocity component, which we proceed to determine formally by χ^2 minimization. We then have a measure of Local Group motion relative to the background frame defined by our distant clusters, which can be compared with Local Group motion within the Local Supercluster itself (e.g., AHMST). Any substantial difference between these two components is presumably caused by a uniform motion of the entire Supercluster relative to other nearby clusters and superclusters.

We next compare our distant cluster Hubble ratios with Virgo and thereby obtain a measure of the Local Group's Virgocentric motion, which can be contrasted again with the velocity field results of AHMST. Good agreement is found between the two independent estimates.

We emphasize that the analysis in this section is independent of scale length, involving only a comparison of Hubble ratios, and not an absolute distance scale. Hence, the uncertainty in zero point of the IR/H I relation does not enter, and, in fact, any arbitrary zero point can be assumed. For convenience we shall retain in the discussion below the zero point adopted previously.

a) Local Group Motion Relative to the 10 Cluster Sample

i) *What Might We Expect?—The* 3 K *Anisotropy*

The search for Local Group motion relative to a scale length greater than that of the Local Supercluster is largely motivated by observations of the dipole anisotropy in the 3 K microwave background radiation. Recent findings in the latter area have come into rather good agreement: First, from the dipole-only solution of Lubin, Epstein, and Smoot (1983), and using a solar-motion correction of 300 sin l cos b, we find a velocity vector of $V = 586$ km s^{-1} toward $\alpha = 10^{\rm h}.44$ and $\delta = -27°.5$. Alternatively, the independent measurements of Fixsen, Cheng, and Wilkinson (1983) lead to a vector of 614 km s^{-1} toward $\alpha = 10^{\rm h}.59$ and $\delta = -24°.7$. The small difference between these two results is within the quoted errors, and is therefore not significant. Note that, following the recommendation of D. Wilkinson, we have used a blackbody temperature of $T = 2.8$ K for these estimates, which brings the Berkeley and Princeton results into even better accord than the conventional $T = 2.7$ K value (cf. Smoot *et al.* 1985; Meyer and Jura 1984; Woody and Richards 1981); the difference leads to a dipole velocity that is lower by $\sim 4\%$. For the following discussion, we shall adopt an average dipole vector of $V = 600 \pm 30$ km s^{-1} toward $\alpha = 10^{\rm h}.5 \pm 0^{\rm h}.2$ and $\delta = -26° \pm 3°$, or, in Galactic coordinates, toward $l = 268°$ and $b = 27°$.

The present-day value of the 3 K dipole vector is roughly twice the magnitude of Virgocentric motion (~ 300 km s^{-1}) found by AHMST and by us (see below), and furthermore lies in a direction some 48° away from M87. This difference between the dipole anisotropy and Local Group motion within the Supercluster is diminished a little if we include the components of the latter motion perpendicular to Virgo measured by AHMST, but it still remains substantial. Given the accuracy with which the 3 K dipole is known, it seems that the effect cannot be fully accounted for by Local Group motion within the Supercluster alone. Rather, an additional motion of ~ 300 km s^{-1} is required, the direction of which, intriguingly enough, is toward our next nearest neighbor supercluster Hydra-Centaurus (cf. Shaya 1984; Sandage and Tammann 1984*a*). However, the question remains as to how large a volume is partaking of such motion. The fact that the residual points toward Hydra-Centaurus is perhaps a hint that the scale size involved is that of the Supercluster itself, instead of a much larger volume which might extend for instance beyond 100 Mpc. If so, in addition to Virgocentric velocity, bulk Supercluster motion should be reflected in the observed Hubble ratios of our 10-cluster sample. The test is a demanding one, though, because at 6000 km s^{-1} we are searching for only a 5% signal. In the following discussion we shall attack the problem using three separate methods.

ii) *Test 1: A Graphical Approach*

We will first demonstrate via graphical means that the large scatter of Hubble ratios for the 10-cluster sample is explained by an unaccounted-for velocity; this will also allow us to obtain a better "feel" for the formalized solution presented further on. We do so by examining what happens to the scatter of the cluster Hubble ratios when a velocity of $\Delta V = 600$ km s^{-1} is applied to the Local Group and allowed to "swing" all around the sky.

Specifically, we compute a figure-of-merit quantity

$$M(\Delta V) \equiv \sum_i |(\langle H_i \rangle - H_i)| ,$$

where $H_i = (V_i + \Delta V \cos \theta_i)/r_i$, and V_i and r_i are the velocities and distances from columns (9) and (5) of Table 6, respectively, while θ_i is the angle between the directed motion ΔV (set at 600 km s^{-1}) and each cluster. The results are shown in Figure 11*a*, where we have plotted the normalized quantity

$$[M(0) - M(600)]/[M(0) - M(600)_{\rm max}]$$

for every 10° step in Galactic latitude and every 20° step in Galactic longitude. Hence, the zero crossing in Figure 11*a* corresponds to those directions in which a 600 km s^{-1} motion leaves the scatter of the cluster Hubble ratios unchanged, while above (below) this line the scatter decreases (increases).

The diagram in Figure 11*a* shows a single, well-defined peak. This implies that, as previously postulated, the large scatter of cluster Hubble ratios in Figure 10*a* is not simply a result of random error. In Figure 10*a* we have distinguished the five distant clusters which lie in the northern galactic hemisphere from the five which lie in the south, and it is clear that the former have Hubble ratios that are systematically smaller. A Virgocentric motion will lead to this effect, but we emphasize that such motion alone does not account for the scatter in the figure. For instance, in units of the adopted zero point, our

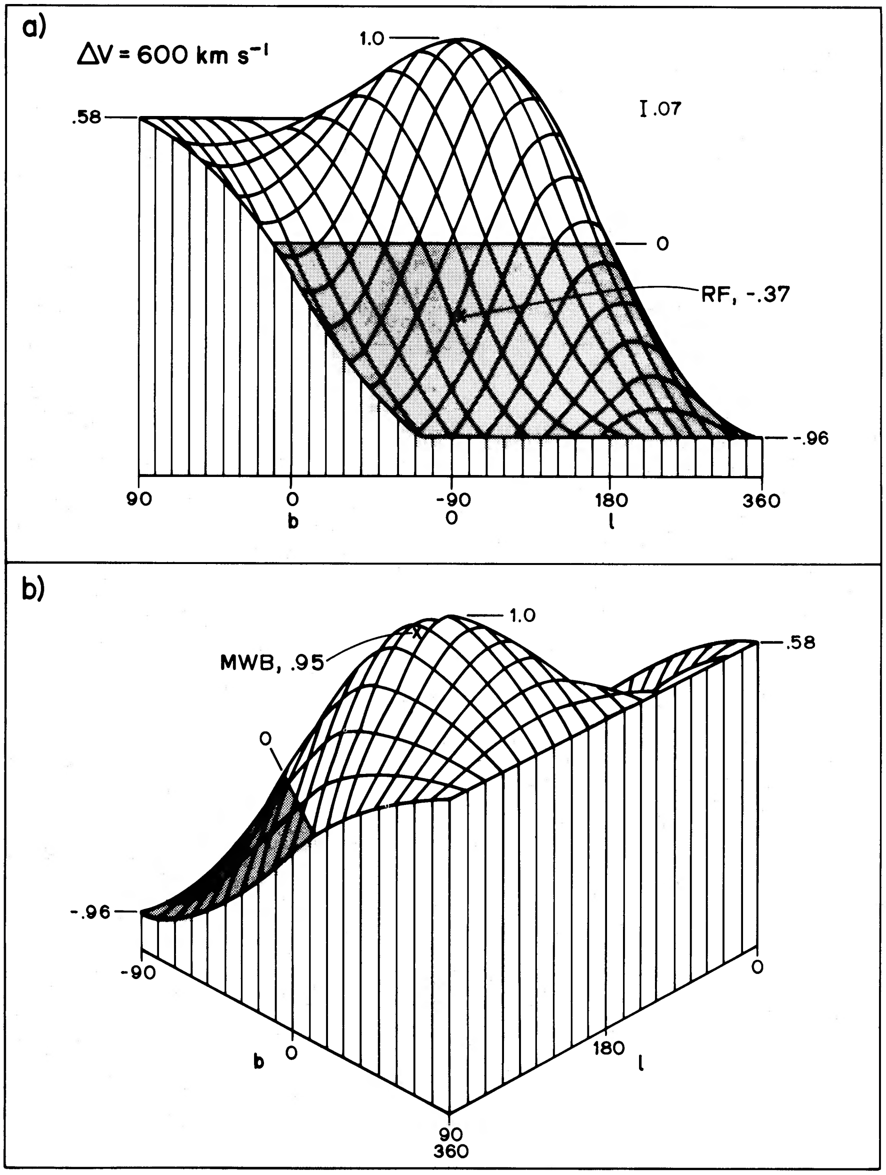

FIG. 11.—(*a*) This diagram illustrates what happens to the scatter of cluster Hubble ratios in Fig. 10*a* when a velocity equal to 600 km s^{-1} is applied to the Local Group and "swung" around the sky. The area above (below) the zero crossing is the location of decreased (increased) scatter. The presence of a single well-defined peak is an indication that the scatter in Fig. 10*a* is not random. The error bar is the typical formal uncertainty in a cluster Hubble ratio (i.e., the peak is significant at the 14 σ level). The cross marks the location of the Rubin-Ford velocity vector (Rubin *et al.* 1976). (*b*) Same as (*a*), with the view rotated 180° and tilted upward 30°. The cross marks the location of the velocity implied by the observed dipole anisotropy in the 3 K microwave background, and lies near the peak of the diagram.

figure of merit $M(0)$ is equal to 69 km s^{-1} Mpc^{-1}, or about 20 times the ~ 3.5 km s^{-1} Mpc^{-1} error of a typical mean cluster Hubble ratio (see Table 6). In contrast, a 300 km s^{-1} Virgo directed motion yields $M(300) = 46$, while the full infall solutions from AHMST (see below) give $M(\text{case } 3.1) = 41$ and $M(\text{case } 5.1) = 40$. By comparison, for the peak in Figure 11*a*, $M_{\max}(600) = 20$, corresponding to a decrease of $\sim 6\ \sigma$ in the scatter over that obtained from the AHMST results alone.

The cross in Figure 11*a* matches the location of the velocity vector found by Rubin *et al.* (1976) in their study of distant Sc I galaxies. The size of this motion was 454 km s^{-1} (not 600), but, even so, our data are inconsistent with the Rubin *et al.* findings at the 3 σ level. On the other hand, the position of the 3 K vector is only $\sim 15°$ from the peak in Figure 11*a*. This location is marked in Figure 11*b*, which is the same diagram rotated 180° and tilted upward 30°.

It may perhaps seem remarkable that we can so adequately determine the vector direction with only 10 test particles, whose positions furthermore are confined to the Arecibo declination range of $\sim 0°$–40°. Indeed, we have been somewhat fortunate in this regard because three of our clusters lay within 14°–35° of the direction anticenter to the 3 K velocity. These three clusters, Pisces, Pegasus, and A2634/66, are the three "high points" in Figure 10*a*, and provide essentially all the "power" to the results in Figure 11 and below. In addition, the magnitude of the velocity vector suggested by our data is in fact not well constrained, owing to the positional degeneracy of the cluster sample. For instance, we have examined contour plots generated by letting ΔV vary from 300 to 1200 km s^{-1}. Over the range 550–950 km s^{-1}, a plateau peak develops as tall and wide as that seen in Figure 11. Even at $\Delta V = 1050$ km s^{-1}, the peak is nearly as high, but it is much sharper and there

TABLE 7

THE cos *A* TEST FOR SUPERCLUSTER MOTION

Cluster	cos *A*	$V_{\rm red}$ (km s^{-1})
Pisces	−0.71	213
A400	−0.18	−288
A539	0.23	−375
Cancer	0.38	−487
A1367	0.32	−120
Coma	0.06	−36
Z74-23	0.15	−364
Hercules	−0.31	628
Pegasus	−0.73	276
A2634/66	−0.86	546

is much less sky area above the zero crossing, and so from a probabilistic standpoint such a high velocity can be excluded.

iii) *Test 2: The* cos *A Method*

A specific test for bulk motion of the Supercluster has been devised by Tammann and Sandage (1985), and it is of interest for comparison's sake to apply it to the present data. First, one corrects the observed cluster velocities to those that would be measured by an observer at the center of the Virgo Cluster. To do this, we adopt a Virgocentric motion of 300 km s^{-1}. Next one assumes that by summing over all clusters in the equation

$$V_{\rm cl} = h_0 r - V_{\rm Super} \cos A ,$$

the second term involving the velocity of the Supercluster and the cosine of the angle between the cluster and the assumed direction of motion will cancel, so that $h_0 = [\sum_i (V_{{\rm cl},i}/r_i)]/N =$ 1368 km sec^{-1} (Virgo distance units)$^{-1}$. One then defines

$$V_{\rm red} = V_{\rm cl} - h_0 r ,$$

which is tabulated in Table 7, and plotted against cos *A* in Figure 12. From the slope of the least-squares fit forced through the origin, we obtain $V_{\rm Super} = 596 \pm 177$ km s^{-1}. This is a 3 σ detection of Local Supercluster motion in the assumed direction $l = 270°$, $b = 5°$. This direction is near the predicted location obtained by subtracting a 300 km s^{-1} Virgocentric velocity from the observed 3 K vector, and the size of the motion is within 1 σ of the expected velocity of $\sim$460 km s^{-1} (see below).

The reader might compare Figure 12 (where the least-squares fit shown has a correlation coefficient of 0.80) with the null results in Figures 3 and 4 from Tammann and Sandage (1985). Even so, we consider this test a less powerful demonstration than the next one, since the results not only are dependent on the assumed Local Group motion within the Supercluster, but also presuppose the direction of Supercluster motion as well.

iv) *Test 3: A Formal Solution*

The formal approach to the problem is to fit the model

$$V_{\rm pred} = H_0 r - \Delta \boldsymbol{V} \cdot \hat{\boldsymbol{r}}$$

to the observed redshifts $V_{\rm obs}$ of the 10 clusters (col. [9] of Table 6). In the above equation, $\boldsymbol{r}$ is the radius vector to any cluster and $\hat{\boldsymbol{r}}$ is the corresponding unit vector. The fit is accomplished by forming the quantity

$$\chi^2 = \sum_{i=1}^{10} \frac{(V_{\rm obs} - V_{\rm pred})^2}{\sigma_V^2 + H_0^2 \sigma_r^2} , \qquad (5)$$

which is then minimized by varying four parameters—the vector $\Delta \boldsymbol{V}$ and H_0. A program kindly made available by J. Tonry was used for this purpose. For σ_V and σ_r, we adopted the quoted errors from columns (9) and (5) of Table 6. Note also that, while the expansion rate is formally solved for, the problem remains scale-free because of the coupling to distance in equation (5).

The solution obtained is $\Delta V = 780 \pm 188$ km s^{-1} toward $l = 255° \pm 17°$ and $b = 18° \pm 13°$, and lies $15° \pm 16°$ in position and 180 ± 190 km s^{-1} in magnitude from our adopted 3 K dipole vector of $\Delta V = 600 \pm 30$ km s^{-1} toward $l = 268° \pm 5°$ and $b = 27° \pm 3°$. *Hence, the difference between the two vectors is not formally significant.* The large magnitude error (which is in good agreement with the graphical estimate

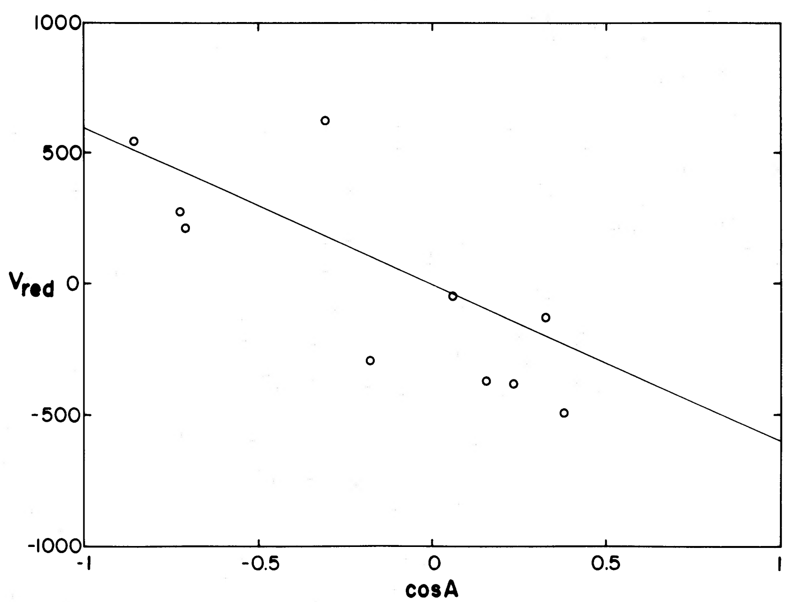

FIG. 12.—The cos *A* test for bulk Supercluster motion (see text for details)

made earlier) is again a result of the positional degeneracy of the sample. For the interested reader, the covariance matrix of the solution is given in the Appendix. We point out here that the reduced χ^2 is $\chi^2/N \sim 1.5/6 \sim 0.25$, implying that our adopted distance and velocity errors are too large. This may be partially because the effectiveness of averaging together the $\langle V \rangle / \langle r \rangle$ and $\langle V/r \rangle$ values from Table 6 is not reflected in those errors. Some support for this notion comes from two alternative χ^2 solutions we have obtained. In the first case, the mean cluster redshifts from Table 1 were adopted, and in the second, each cluster galaxy was individually treated so that a solution from 148 rather than only 10 test particles was determined. In both instances results similar to our initial solution were achieved, but with errors and χ^2 values roughly double in size.

We have also determined a solution using the YST solar motion correction to the centroid of the Local Group (see de Vaucouleurs and Peters 1981 for another version of the correction). For this purpose, the mean redshifts in column (9) of Table 6 require an adjustment which is listed in Table 8. From the small size of these corrections we do not anticipate a large change, and in fact the new solution yields a velocity $\Delta V = 728 \pm 252$ km s^{-1} toward $l = 255°$ and $b = 26°$, in comparison with the similarly adjusted dipole vector of $V = 616$ km s^{-1} toward $l = 276°$ and $b = 30°$. The difference in position and magnitude is now $19° \pm 16°$ and 112 ± 254 km s^{-1}, and is again not statistically significant.

TABLE 8

ADJUSTMENTS TO MEAN CLUSTER VELOCITIES[a]

Cluster	ΔV (km s^{-1})
Pisces	58
A400	81
A539	85
Cancer	48
A1367	−21
Coma	−39
Z74-23	−66
Hercules	−76
Pegasus	23
A2634/66	32
Virgo	−40

[a] Using YST centroid solution.

v) *Decomposition of the* 3 K *Motion*

In view of the above results, we believe the motion giving rise to the 3 K anisotropy has now been conclusively detected. Furthermore, it appears that the dipole velocity can be understood as the sum of two principal components, the first due to Local Group motion within the Local Supercluster, and the second to bulk Supercluster motion as a whole. In this section we examine possible decompositions of the 3 K dipole into these two components.

For our purpose we must have independent knowledge of Local Group movement within the Supercluster. We begin by noting that such motion is itself the potential sum of several components. These include, first, the infall velocity to Virgo, that is, the motion that results from gravitational attraction of the Virgo Cluster at the distance of the Local Group.[6] Second, there is the peculiar motion of the Local Group itself. Finally, there may be rotation of the Supercluster as a whole.[7] In what follows we shall make considerable use of the AHMST analysis, the sole study available which treats the various Local Group components separately.

Specifically, we consider two AHMST solutions, case 3.1 and case 5.1, which are believed to be minimally biased, and which differ only in that the latter (unlike the former) allows the Supercluster to rotate. However, we must first adjust the AHMST results to the new Virgo redshift used here. To do so, we can use Figure 5*c* from AHMST, which illustrates the change in Virgocentric motion as the Virgo Cluster redshift is varied over the range 919–1119 km s^{-1}. This figure indicates that for a 55 km s^{-1} increase in redshift we must decrease the AHMST motion toward Virgo by (only) 10 km s^{-1} (the perpendicular components are assumed unaffected). Note that the change is so small because AHMST actually detected the dipole pattern in the Supercluster velocity field, and their results were thus little weighted by the Virgo redshift itself. In contrast, the Virgocentric motion derived in Paper III and also here further below couples directly with the Virgo radial velocity.

For illustrative purposes, in addition to the two AHMST solutions we will consider a third possibility (referred to as "case 6"), which simply involves a 300 km s^{-1} Virgocentric motion of the Local Group with no perpendicular components. The three alternative decompositions are summarized in Table 9, where we have employed two coordinate systems: Galactic coordinates (l, b) and the (x, y, z) system of AHMST. In the latter, z points toward M87, and y points roughly toward the supergalactic pole. For the interested reader, the transformation matrix between (l, b) and (x, y, z) is given in the Appendix.

We should also again consider what happens if the YST centroid correction is adopted. The Virgo redshift would then become 1033 km s^{-1}, which is close to the value of 1019 km s^{-1} used by AHMST. We will then assume that use of the YST correction would be directly reflected as a change in the peculiar components of Local Group motion (an assertion which to be fully proved requires redoing the AHMST analysis). The appropriate corrections to cases 3.1 and 5.1 are $\Delta w_x = 47$ km s^{-1}, $\Delta w_y = 63$ km s^{-1}, and $\Delta w_z = 40$ km s^{-1}, and the various decompositions obtained after applying these adjustments are also listed in Table 9. Because there is little change in relative space velocities of the 3 K dipole and Local Group motion within the Supercluster, adopting the YST centroid correction makes only a very small difference to the resulting bulk Supercluster motion (see Table 9).[8]

vi) *Discussion*

The results in Table 9 indicate that the motion of the Supercluster probably ranges between 300 and 450 km s^{-1}. The directions of motion toward $l \sim 270°$ and $b \sim 0°$ are roughly

[6] Strictly speaking, one should measure infall to the mass center of the Local Supercluster, but we shall assume for the discussion at hand that this point is synonymous with the Virgo Cluster center.

[7] Other ordered motions—for example, of galaxy clouds within the Supercluster—may also exist, but we assume that these are irrelevant to the present problem.

[8] Tammann and Sandage (1985) have also attempted to adjust the AHMST results to the YST centroid, but they have incorrectly subtracted rather than added 40 km s^{-1} to the Virgocentric motion, apparently confusing the observed velocity of other galaxies with the velocity of the Local Group itself. Hence, their statement that the peculiar Local Group motion toward Virgo is reduced to an "insignificant amount" is wrong, and in fact the significance of this component appears to substantially increase with the YST correction.

TABLE 9

DECOMPOSITION OF THE DIPOLE ANISOTROPY[a]

Vector Motion	V_T (km s^{-1})	$w_x^{\mathrm{tot}\ \mathrm{b}}$ (km s^{-1})	$w_y^{\mathrm{tot}\ \mathrm{b}}$ (km s^{-1})	$w_z^{\mathrm{tot}\ \mathrm{b}}$ (km s^{-1})	l	b
3 K	600	268 ± 30	−358 ± 30	400 ± 30	268°	27°
	(616)	(315)	(−295)	(440)	(276)	(30)
Present work	780 ± 188	266	−611	406	255 ± 17	18 ± 13
	(728)				(255)	(26)
Rubin *et al.* 1976	454	−377	−207	−144	163	−11
Local Group motion within Supercluster:						
Case 3.1	357	−65 ± 40	−143 ± 48	321 ± 41[c]	...	...
	(380)	(−18)	(−80)	(371)		
Case 5.1	333	74 ± 71	−141 ± 47	293 ± 39[c]	...	...
	(372)	(121)	(−78)	(343)		
Case 6[d]	300	≡0	≡0	300 ± 40	...	...
Supercluster motion:						
3 K—case 3.1	404	333 ± 50	−215 ± 57	79 ± 51	285	−4
	(402)			(69)	(285)	(−6)
3 K—case 5.1	310	194 ± 77	−217 ± 56	107 ± 49	270	5
	(307)			(97)	(271)	(3)
3 K—case 6	458	268 ± 30	−358 ± 30	100 ± 50	265	−2
	(454)	(315)	(−295)	(140)	(275)	(3)
3 K—Rubin *et al.* 1976	857	645	−151	544	...	...

[a] Values in parentheses under main entries are estimated results of using the Yahil, Sandage, and Tammann 1977 centroid correction in place of 300 sin l cos b.

[b] These are the components of motion in the coordinate system used by AHMST; z points toward M87, and y points roughly near the supergalactic pole.

[c] These values have been revised for the new redshift of Virgo adopted since AHMST.

[d] See text (not considered by AHMST).

comparable in the three instances considered. As noted earlier, this direction is close (~25°) to the Hydra-Centaurus Supercluster at $l \sim 285°$ and $b \sim 25°$. In Figure 13 we specifically illustrate the decomposition of the 3 K dipole for case 5.1.

The bulk Supercluster motion is similar in size to Local Group motion within the Supercluster itself, which raises an interesting point. The most natural explanation of the bulk motion involves gravitational attraction of Hydra-Centaurus. This supercluster, at a redshift $\gtrsim 3000$ km s^{-1}, must then contain $\gtrsim 4$ times the mass of the Local Supercluster. The presence of this much matter is by no means clear, at least in visible form, nor apparently is it obvious in *IRAS* source counts (Davis 1985). Because of the low Galactic latitude and location in the south, there is today little detailed knowledge of Hydra-Centaurus; indeed, it was not long ago that Chincarini and Rood (1979) recognized the structure as our nearest neighbor supercluster. Hopp and Materne (1985) appear to have found a connecting bridge between the Local Supercluster and

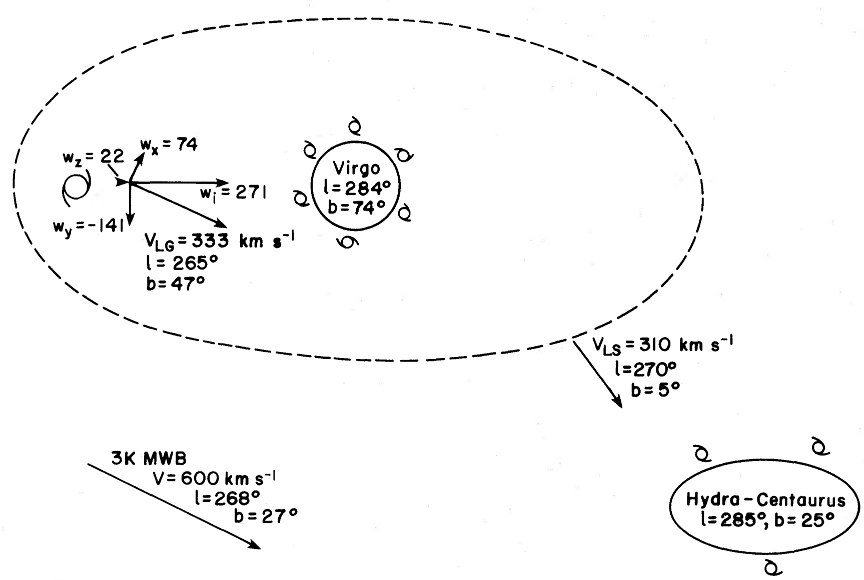

FIG. 13.—Schematic decomposition of the dipole anisotropy into its principal components: Local Group motion within the Supercluster, dominated by gravitational infall toward Virgo; and bulk motion of the entire Supercluster, the direction of which lies close to the nearby Hydra-Centaurus Supercluster.

Hydra-Centaurus. Furthermore, the latter may in reality be the tip of a much larger filamentary entity extending through the Galactic plane and encompassing the Telescopium-Pavo-Indus Supercluster as well (Fairall 1985; Kraan-Korteweg 1985). This extension, however, runs off toward higher Galactic latitudes in a direction relative to Hydra-Centaurus that is away from the location of the bulk Supercluster motion indicated in Table 9. This may not be surprising, though, since there are other nearby superclusters (e.g., Perseus-Pisces, Coma) which might be expected to have some influence on Local Supercluster motion as well, for example, keeping this motion from pointing "directly at" Hydra-Centaurus. The whole problem requires further study.

In principle, our data could also be used to measure the bulk motions of the 10 clusters in the sample. However, the expected typical signal would be only $\sim 350/3^{1/2} \sim 200$ km s^{-1}, where the additional factor $3^{1/2}$ is needed because we can only observe the one-dimensional component. In practice the test cannot be made, owing to the value of reduced $\chi^2 < 1$ obtained earlier. The data do suggest (see Fig. 12) that supercluster motions are constrained to values less than 500 km s^{-1}, an important result. Unless we have an unusually small bulk motion, such a limit is also necessarily implied by the size of the 3 K dipole vector itself. Further study of supercluster-supercluster interactions is clearly going to provide us with valuable information about galaxy formation processes and the size and number density of large mass scales in the universe (e.g., Shaya 1984; Vittorio and Silk 1985).

In this regard, it would be particularly important to pin down our Local Group motion better relative to various extragalactic frames. Especially useful would be good IR/H I distances to the Hydra and Centaurus clusters themselves, since this would largely eliminate the aforementioned degeneracy of our data introduced by confinement to the Arecibo declination range. Unfortunately, the present-day lack of a large southern hemisphere radio telescope comparable to Arecibo will hinder collection of the high signal-to-noise H I profiles that are required (cf. Richter and Huchtmeier 1983).

Two other recent studies have found good agreement between the 3 K dipole vector and Local Group motion relative to an exterior Supercluster frame. The first, by Hart and Davies (1982), used as a standard candle H I fluxes for a morphologically similar sample of distant spirals. However, these results must be viewed with caution because the authors have yet to publish their data. In the second work, de Vaucouleurs and Peters (1984) employ four different distance indicators for a sample of ~ 600 nearby galaxies with redshifts $V < 4000$ km s^{-1}. Their estimated uncertainties are comparable in size to those obtained here. Unfortunately, there is a problem in this study in that de Vaucouleurs and Peters have chosen to ignore the Virgocentric flow, which must render their solutions invalid within 3000 km s^{-1}, although their most distant 100 galaxy subset does appear to reflect motion toward the microwave background.

b) *The Virgocentric Motion*

By comparing our distant cluster Hubble ratios to that for Virgo itself, we can obtain an independent estimate for the Virgocentric motion of the Local Group. As already noted, this motion is the sum of Local Group peculiar velocity toward Virgo and gravitational infall. An important aspect of the latter quantity is that it provides a direct and very strong local constraint on the cosmological mass density parameter Ω (see AHMST and references therein).

Taking explicit account of the bulk Supercluster motion, we can derive an estimate of Virgocentric motion ΔV from each of our clusters, using the equation

$$\Delta V = \{\Delta H + [V'(\cos \phi)/r_{\rm cl}]\}/\{(1/r_{\rm Vg}) - [(\cos \theta)/r_{\rm cl}]\} .$$

In this expression, V' is the Supercluster motion which makes an angle ϕ with the direction of the distant cluster, θ is the angle between Virgo at distance $r_{\rm Vg}$ and the distant cluster at $r_{\rm cl}$, and ΔH is the difference in observed Hubble ratio between the two. We have considered two cases. In the first we set $V' = 0$ (i.e., no Supercluster motion) and reproduce the calculation of Paper III. In the second, we take the Supercluster motion to be 310 km s^{-1} toward $l = 270°$, $b = 5°$ (see Table 9).

The results are summarized in Table 10. Without Supercluster motion, a mean of $\Delta V = 287 \pm 25$ km s^{-1} is found, while allowing the Supercluster to move yields $\Delta V = 281 \pm 17$ km s^{-1}. The close agreement between the two estimates is not unanticipated because, first, our 10 "test particles" are about evenly distributed in a great circle around the sky, and, second, the Supercluster motion is not large with respect to the cluster velocities. Nevertheless, the scatter in ΔV values is, as expected, considerably diminished when the Supercluster motion is allowed for. However, the quoted formal errors are obvious lower limits which do not, for instance, reflect the observed ± 38 km s^{-1} uncertainty in the Virgo redshift. This points up the aforementioned weakness of the present method compared with the AHMST results, which are largely independent of Virgo velocity.

Our estimate of Virgocentric motion nonetheless agrees very well with the AHMST findings, which place this quantity between 290 and 320 km s^{-1} (see Table 9). The AHMST analysis shows that the motion is dominated not by peculiar Local Group velocity but by gravitational infall in the range 240–270 km s^{-1}, a (small) amount which implies that the universe is far from closure density.

We emphasize that the present results supersede the initial study of Paper III based on only four distant clusters, where as previously discussed a substantially larger ΔV value of 480 ± 75 km s^{-1} had been derived. The decrease in ΔV of ~ 190 km s^{-1} now obtained can be attributed to the following four factors: (1) the change in Virgo redshift from Paper II (55

TABLE 10

Virgocentric Motion from Relative Cluster Distance Moduli

Cluster	ΔV_1[a] (km s^{-1})	ΔV_2[b] (km s^{-1})
Pisces	345	294
A400	249	241
A539	239	250
Cancer	153	188
A1367	260	289
Coma	285	290
Z74-23	200	239
Hercules	382	369
Pegasus	373	310
A2634/66	378	338
Mean	287 ± 25	281 ± 17

[a] This estimate assumes that the Local Supercluster is stationary.

[b] This estimate assumes a Supercluster motion of $V = 310$ km s^{-1} toward $l = 270°$ and $b = 5°$.

km s^{-1}); (2) the increase in both the quantity (148 galaxies within 10 clusters instead of 38 within four clusters) and quality of the cluster data sample ($\sim$55 km s^{-1}); (3) the diameter corrections discussed in § IV ($\sim$70 km s^{-1}); and (4) the change from a linear to a quadratic form of the IR/H I relation ($\sim$10 km s^{-1}).

One additional estimate of the Virgocentric motion can be obtained from the following argument: In the next section of the paper we derive a global value for H_0 which, in combination with our Virgo distance, implies a cosmological redshift for the cluster of 1350 ± 75 km s^{-1}. The observed redshift of 1073 ± 38 km s^{-1} then immediately leads to $\Delta V = 277 \pm 84$ km s^{-1}, in good agreement with the previous results. (Note that other recent but low-weight estimates of Virgocentric motion can be found in Tammann and Sandage 1985.)

Finally, we once again consider the effects of applying the YST solar-motion correction to the centroid of the Local Group. The principal difference will be to decrease the Virgo redshift by 40 km s^{-1} (see Table 8) to 1033 km s^{-1}. This will in turn increase by $\sim$40 km s^{-1} the estimates of Virgocentric motion derived here to $\sim$320–330 km s^{-1}. Similar adjustment of the AHMST results leads to values for ΔV in the range 340–370 km s^{-1} (see Table 9).

To summarize, the available evidence from several differing applications of the IR/H I relation suggests a Virgocentric motion of $\sim$300 km s^{-1}.

VII. THE GLOBAL VALUE OF THE HUBBLE CONSTANT

A global value for H_0 follows immediately upon correcting our distant clusters for the 3 K dipole effect and/or Virgo for Local Group motion within the Supercluster. The velocity corrections are listed in column (10) of Table 6, and the resulting Hubble ratios are given in column (11). The latter are plotted in Figure 10*b*, and it can be seen that the scatter in Figure 10*a* has virtually disappeared. The velocity-distance relation for the entire 11-cluster sample is illustrated in Figure 14. It is again apparent that these data leave little room for non-Hubble supercluster motions that are larger than $\sim$500 km s^{-1}.

The formal value obtained by averaging the 11-cluster Hubble ratios is $H_0 = 92 \pm 1$ km s^{-1} Mpc^{-1}. The zero-point uncertainty has of course not been included in the error estimate. In fact, the Sandage-Tammann calibrators in Figure 8*a* lead to $H_0 = 74$ km s^{-1} Mpc^{-1}, while the de Vaucouleurs calibrators in Figure 8*b* give $H_0 = 100$ km s^{-1} Mpc^{-1}, a range that can be plausibly interpreted as defining the current true uncertainty in the expansion rate. A critical role for the Hubble Space Telescope will be to provide Cepheid distances for a large sample of nearby galaxies so that a reliable zero point to the IR/H I relation can finally be derived.

Ignoring Virgo for the moment, we note that with our adopted zero point the five nearest clusters yield $H_0 = 91 \pm 1$, while the five most distant ones give $H_0 = 94 \pm 1$. This small difference could conceivably result from a residual Malmquist-like bias, but any such effect is clearly inconsequential. We also note that the five clusters with the smallest surface brightness residuals from Table 3 (only four of which are among the five closest clusters) yield $H_0 = 93 \pm 1$, while the five clusters having the largest residuals give $H_0 = 92 \pm 2$. Again, we find no evidence for any substantial bias introduced because of the systematic differences in mean cluster surface brightness properties.

Finally, we note the lack of any obvious environmental factors. In particular, for the prototypical dense, spiral-poor Coma Cluster we find a Hubble ratio of $H_0 = 93$, a value essentially identical with the mean of the whole cluster sample. For several reasons, we do not consider this result surprising. First, as previously noted, our cluster objects (and particularly Coma) tend to be weighted by spirals outside the central cores. (For Virgo, Tully and Shaya 1984 have in fact made the intriguing suggestion that such systems are now just falling into the cluster for the first time.) Although evidence does exist for H I deficiency in some of our clusters (e.g., Giovanelli 1985; Haynes, Giovanelli, and Chincarini 1984; Bothun, Schommer, and Sullivan 1984), the effect is found primarily inside the central regions.

As an example, we refer to Figure 1 of Giovanelli (1985), and note that there is no difference in Hubble ratio between our H I–deficient clusters (Virgo, Coma, and A1367) and nondeficient clusters (Pegasus, Cancer, Z74-23, and A2151). Perhaps more to the point, a search for deficiencies among the specific

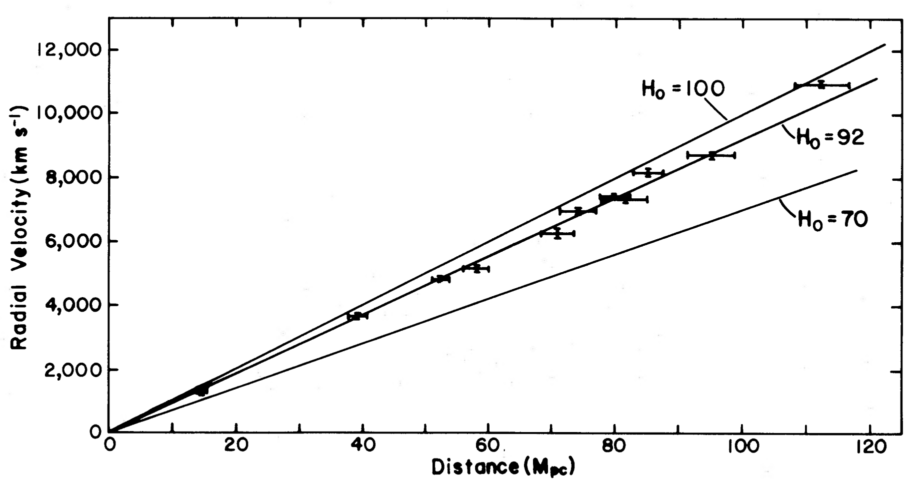

FIG. 14.—Velocity-distance relation for 11 galaxy clusters, after correction for all Local Group streaming motion. The expansion rate is linear to within the measurement errors. The outer lines may be taken as a measure of the current acceptable range in H_0 arising from uncertainty in distances to nearby calibrating galaxies.

cluster members used in this paper was undertaken by Bothun *et al.* (1985*b*), with null results. We stress further that to affect our distances significantly one must not simply lower the gaseous content, but must truncate the H I at a point interior to where the galaxy rotation curve would otherwise flatten out. Even in Coma, it remains unclear to what extent such a drastic process has ever occurred.

Befor closing this section, we feel compelled to respond to a number of misconceptions concerning the luminosity/line-width method raised in recent papers by Sandage and Tammann. These authors consider the method "promising but not mature." They emphasize that results obtained in the blue, particularly by Richter and Huchtmeier (1984), appear to give a small value for the expansion rate. In Sandage and Tammann (1984*a*), the reliability of the infrared data is questioned because of the fact that the photometry is obtained by chopping. Nevertheless, Sandage and Tammann (1984*b*) argue that the IR/H I method also leads to a low expansion rate. Elsewhere (Sandage and Tammann 1984*c*, 1985), these authors again imply that the method is uncertain either because different wavelengths yield different distances, or because treatment of the same data by various authors yields differing results (an argument which it seems to us can be applied to virtually every present-day distance indicator).

To begin with, there is a major problem with the Richter and Huchtmeier (1984) study in that they include galaxies with an inclination less than 45°. As discussed by Aaronson, Huchra, and Mould (1979), this results in a systematic bias toward large distances, probably arising from a tendency to underestimate increasingly the inclination of face-on galaxies because of spiral arms opening along the minor axis. The effect is easily visible in Richter and Huchtmeier's data: for example, of the 66 Virgo galaxies in their Table 2, the 22 having $i < 45°$ yield a mean modulus that is 0.49 ± 0.26 mag larger than the mean modulus obtained from the remaining 44 galaxies having $i \geq 45°$, independent of which of the two calibrating relations offered by Richter and Huchtmeier is employed. In view of this point, Richter and Huchtmeier's entire calibration procedure must be cast into doubt.

Using their own calibration, Sandage and Tammann (1984*b*) analyze the Richter and Huchtmeier data and obtain a Virgo modulus of 31.66 mag. This value, however, must be decreased by ~ 0.1 mag because of the aforementioned inclination problem. With the same set of calibrating distances applied to our infrared data, Sandage and Tammann (1984*b*) derive a Virgo modulus of 31.47 mag, which is only ~ 0.1 mag different from the (corrected) result obtained using the blue data. Hence, *as long as the calibrator moduli are kept the same, there is no significant wavelength dependence in the relation.* A similar conclusion has been reached by Bottinelli *et al.* (1984; see also Tully and Shaya 1984). However, because of the very large and uncertain internal absorption corrections to the blue magnitudes, the IR results must be accorded much higher weight.

Using the (older) Sandage-Tammann distances quoted in Paper IV, the IR data from Aaronson *et al.* (1982*b*), and our new quadratic form of the IR/H I relation, we derive a Virgo modulus of 31.31 mag (which for reasons discussed earlier is ~ 0.1 mag larger than the result obtained from the Paper IV linear relation). This remaining difference of ~ 0.15 mag from the Sandage and Tammann (1984*b*) result is due largely to the new and anomalously large distances these authors have adopted for M81 and especially M33. The point of all this is to emphasize that *our primary difference with Sandage and Tammann rests in the distances to the calibrating galaxies*, and not elsewhere. In particular, with our preferred zero point from Figure 7, we obtain a "best guess" Virgo modulus of 30.82 mag.

Now Sandage and Tammann (1984*b*) go on to derive a Hubble constant near 50 by adopting a relative Virgo-Coma modulus of 3.92 mag, *based not on the* IR/H I *method*, but on a variety of other techniques. We believe that this relative modulus, which differs from the one here in Table 6 by 0.23 mag, is too large. In particular, we again note the excellent agreement between our own results and the velocity dispersion measurements of Dressler (1984). Furthermore, the Virgocentric motion implied by the larger relative modulus is only 79 km s^{-1}, or 119 km s^{-1} if the YST centroid correction is used.[9] In either case these values are considerably less than even Sandage and Tammann's own stated preference for a 220 km s^{-1} infall, and can only be reconciled by making the ad hoc assumption that the cluster velocities in Table 1 are in substantial error.

Finally, we note that Sandage and Tammann's (1984*a*) suggestion of a bias with distance in our results because of reference-beam problems is unfounded. First, the variation in relative chopper throw does not differ between large and small galaxies as they claim, because in making the measurements we move from small to large telescopes. In fact, most of the observations in this series of papers have been secured with the identical large-throw IR photometer, and precisely because we look at edge-on spirals, the chopping is in many instances completely off the galaxy. Sandage and Tammann's statement to the contrary is again incorrect. Even in the cases when reference-beam flux is present, the necessary correction is both well determined and *small*, being typically in the range 0.01–0.03 mag, and very rarely exceeding 0.05 mag.

VIII. SUMMARY

In this paper we have employed the IR/H I relation to derive relative distances to 10 nearby galaxy clusters. We have along the way identified and addressed several selection biases in the data set. The final cluster Hubble ratios exhibit considerable scatter, signifying the presence of an unaccounted for Local Group streaming motion. Formal solution leads to a velocity in close agreement with the 3 K dipole anisotropy, which can now be understood to arise from two principal components—Local Group motion within the Supercluster, and bulk motion of the Supercluster itself. Both components are ~ 300 km s^{-1} in size. An unassailable value for the expansion rate remains beyond our grasp, owing to continuing problems with nearby galaxy distances. We believe the best current evidence favors a large value for the Hubble constant, $H_0 \sim 90$ km s^{-1} Mpc^{-1}, but the issue cannot be put to rest until after the launch of the Hubble Space Telescope.

It is a pleasure to thank Helen Bluestein for her cheerful and diligent typing of several lengthy manuscript drafts. We also acknowledge M. Kun for use of computing facilities, and the Lotus Corporation for some marvelous software. This study was partially supported with funds from NSF grants AST 83-16629 and AST 83-06139.

[9] The Supercluster motion has been ignored in these estimates, but this will have little effect, since the motion lies in a direction nearly 90° from Coma.

APPENDIX

In § VI we used a four-parameter fit to obtain a solution for Local Group motion relative to the frame defined by our cluster sample. So that P. Schechter and other possibly interested readers can see how the various parameters couple, the covariance matrix of the solution is given in Table 11.

Also, for the reader's benefit we present below the transformation matrix between Galactic coordinates and the (x, y, z) system employed here and by AHMST:

$$\begin{pmatrix} x \\ y \\ z \end{pmatrix} = \begin{pmatrix} 0.73384 & -0.64216 & -0.22158 \\ 0.67632 & 0.72123 & 0.14969 \\ 0.06369 & -0.25971 & 0.96358 \end{pmatrix} \begin{pmatrix} \cos l \cos b \\ \sin l \cos b \\ \sin b \end{pmatrix} .$$

TABLE 11

COVARIANCE MATRIX

Parameter	V_x	V_y	V_z	h_0
V_x	1	−0.46	−0.75	−0.88
V_y	...	1	0.46	0.42
V_z	...	...	1	0.64
h_0	...	...	...	1

REFERENCES

Aaronson, M. Huchra, J., and Mould, J. 1979, *Ap. J.*, **229**, 1.
Aaronson, M., Huchra, J., Mould, J., Schechter, P. L., and Tully, R. B. 1982*a*, *Ap. J.*, **258**, 64 (AHMST).
Aaronson, M., *et al.* 1982*b*, *Ap. J. Suppl.*, **50**, 241.
Aaronson, M., and Mould, J. 1983, *Ap. J.*, **265**, 1 (Paper IV).
Aaronson, M., Mould J., and Huchra, J. 1980, *Ap. J.*, **237**, 655 (Paper I).
Aaronson, M., Mould, J., Huchra, J., Sullivan, W. T., Schommer, R. A., and Bothun, G. D. 1980, *Ap. J.*, **239**, 12 (Paper III).
Balona, L. A., and Shobbrook, R. R. 1984, *M.N.R.A.S.*, **211**, 375.
Beers, T. 1985, private communication.
Blanco, V. M., and Blanco, B. M. 1985, in *Proc. Frascati Workshop on Population II Variables*, in press.
Bosma, A. 1985, *Astr. Ap.*, **149**, 482.
Bothun, G. D., Aaronson, M., Schommer, R., Huchra, J., and Mould, J. 1984*a*, *Ap. J.*, **278**, 475.
Bothun, G. D., Aaronson, M., Schommer, R., Mould, J., Huchra, J., and Sullivan, W. T. 1985*a*, *Ap. J. Suppl.*, **57**, 473.
Bothun, G. D., Geller, M. J., Beers, T. C., and Huchra, J. P. 1983, *Ap. J.*, **268**, 47.
Bothun, G. D., Mould, J. R., Schommer, R. A., and Aaronson, M. 1985*b*, *Ap. J.*, **291**, 586.
Bothun, G. D., Romanishin, W., Strom, S. E., and Strom, K. M. 1984*b*, *A.J.*, **89**, 1300.
Bothun, G. D., Schommer, R. A., and Sullivan, W. T. 1984, *A.J.*, **89**, 466.
Bottinelli, L., Gouguenheim, L., Paturel, G., and de Vaucouleurs, G. 1983, *Astr. Ap.*, **118**, 4.
———. 1984, *Astr. Ap. Suppl.*, **56**, 381.
Bottinelli, L., Gouguenheim, L., Paturel, G., and Teerikorpi, P. 1985, preprint.
Caldwell, J. A. R. 1983, *Observatory*, **103**, 244.
Chincarini, G. L., Giovanelli, R., and Haynes, M. P. 1979, *A.J.*, **84**, 1500.
———. 1983, *Ap. J.*, **269**, 13.
Chincarini, G. L., Giovanelli, R., Haynes, M., and Fontanelli, P. 1983, *Ap. J.*, **267**, 511.
Chincarini, G. L., and Rood, H. J. 1979, *Ap. J.*, **230**, 648.
Cohen, J. C. 1985, *Ap. J.*, **292**, 90.
Cornell, M. E. Aaronson, M., Bothun, G., and Mould, J. 1985, in preparation.
Davis, M. 1985, private communication.
de Vaucouleurs, G., de Vaucouleurs, A., and Corwin, H. G. 1976, *Second Reference Catalogue of Bright Galaxies* (Austin: University of Texas Press) (RC2).
de Vaucouleurs, G., and Peters, W. L. 1981, *Ap. J.*, **248**, 395.
———. 1984, *Ap. J.*, **287**, 1.
Dressler, A. 1984, *Ap. J.*, **281**, 512.
Fairall, A. P. 1985, preprint.
Feast, M. W. 1985, *M.N.R.A.S.*, **211**, 51P.
Fernie, J. D., and McGonegal, R. 1983, *Ap. J.*, **275**, 732.
Fixsen, D. J., Cheng, E. S., and Wilkinson, D. T. 1983, *Phys. Rev. Letters*, **50**, 620.
Freedman, W. L. 1985, in *IAU Colloquium 82, Cepheids: Observation and Theory*, ed. B. F. Madore (Cambridge: Cambridge University Press), p. 225.
Frenk, C. S., and White, S. D. M. 1982, *M.N.R.A.S.*, **198**, 173.
Giovanelli, R. 1985, in *ESO Workshop on the Virgo Cluster*, ed. O.-G. Richter and B. Binggeli (Garching: ESO), p. 67.
Giovanelli, R., Chincarini, G. L., and Haynes, M. P. 1981, *Ap. J.*, **247**, 383.
Hart, L., and Davies, R. D. 1982, *Nature*, **297**, 191.
Haynes, M. P., and Giovanelli, R. 1984, *A.J.*, **89**, 758.
Haynes, M. P. Giovanelli, R., and Chincarini, G. L. 1984, *Ann. Rev. Astr. Ap.*, **22**, 445.
Hopp, U., and Materne, J. 1985, *Astr. Ap. Suppl.*, **61**, 93.
Huchra, J. 1984, in *ESO Workshop on the Virgo Cluster*, ed. O.-G. Richter and B. Binggeli (Garching: ESO), p. 181.
———. 1985, in preparation.
Kraan-Korteweg, R. C. 1983, *Astr. Ap.*, **125**, 109.
———. 1985, in preparation.
Lewis, B. M. 1983, *A.J.*, **88**, 962.
———. 1984, *Ap. J.*, **285**, 453.
Lubin, P. M., Epstein, G. L., and Smoot, G. F. 1983, *Phys. Rev. Letters*, **50**, 616.
Madore, B. F. 1985, private communication.
Madore, B. F., and Freedman, W. L. 1985, private communication.
Madore, B. F., McAlary, C. W., McLaren, R. A., Welch, D. L., Neugebauer, G., and Matthews, K. 1985, *Ap. J.*, **294**, 560.
Maucherat, A. J., Dubout-Crillon, R., Monnet, G., and Figon, P. 1984, *Astr. Ap.*, **133**, 341.
McAlary, C. W., and Welch, D. L. 1985, in *IAU Colloquium 82, Cepheids: Observation and Theory*, ed. B. F. Madore (Cambridge: Cambridge University Press), p. 228.
McGonegal, R., McLaren, R. A., McAlary, C. W., and Madore, B. F. 1982, *Ap. J. (Letters)*, **257**, L33.
Menzies, J. W., and Whitelock, P. A. 1985, *M.N.R.A.S.*, **212**, 783.
Meyer, D. M., and Jura, M. 1984, *Bull. AAS*, **16**, 1014.
Mould, J., Aaronson, M., and Huchra, J. 1980, *Ap. J.*, **238**, 458 (Paper II).
Mould, J. R., and Kristian, J. 1985, *Ap. J.*, submitted.
Nilson, P. 1973, *Uppsala General Catalogue of Galaxies* (*Uppsala Astr. Obs. Ann.*, Vol. **6**) (UGC).
Peterson, B. M., Strom, S. E., and Strom, K. M. 1979, *A.J.*, **84**, 735.
Pierce, M. J., and Tully, R. B. 1984, *Bull. AAS*, **16**, 950.
Richter, O.-G., and Huchtmeier, W. K. 1982, *Astr. Ap.*, **109**, 155.
———. 1983, *Astr. Ap.*, **125**, 187.
———. 1984, *Astr. Ap.*, **132**, 253.
Roberts, M. S. 1978, *A.J.*, **83**, 1026.
Rubin, V. C., Burstein, D., and Thonnard, N. 1980, *Ap. J. (Letters)*, **242**, L149.
Rubin, V. C., Ford, W. K., Jr., Thonnard, W., and Burstein, D. 1982, *Ap. J.*, **261**, 439.
Rubin, V. C., Thonnard, N., Ford, W. K., Jr., and Roberts, M. S. 1976, *A.J.*, **81**, 719.
Sandage, A., and Carlson, G. 1983, *Ap. J. (Letters)*, **267**, L25.
Sandage, A., and Humphreys, R. H. 1980, *Ap. J. (Letters)*, **236**, L1.
Sandage, A., and Tammann, G. A. 1984*a*, in *Large-Scale Structure of the Universe, Cosmology and Fundamental Physics*, ed. G. Setti and L. Van Horn (Geneva: CERN), p. 127.
———. 1984*b*, *Nature*, **307**, 326.
———. 1984*c*, in *Supernovae as Distance Indicators*, ed. N. Bartel (Berlin: Springer), p. 1.
———. 1985, preprint.
Schmidt, E. G. 1984, *Ap. J.*, **285**, 801.
Schommer, R. A., Olszewski, E. W., and Aaronson, M. 1984, *Ap. J. (Letters)*, **285**, L53.
Shaya, E. J. 1984, *Ap. J.*, **280**, 470.
Skillman, E. 1985, Ph.D. thesis, University of Washington.
Smoot, G. F., *et al.* 1985, *Ap. J. (Letters)*, **291**, L23.

Tammann, G. A., and Sandage, A. 1968, *Ap. J.*, **151**, 825.
———. 1985, *Ap. J.*, **294**, 81.
Teerikorpi, P. 1984, *Astr. Ap.*, **141**, 407.
Tully, R. B., and Fisher, J. R. 1977, *Astr. Ap.*, **54**, 661.
Tully, R. B., and Fouqué, P. 1985, *Ap. J. Suppl.*, **58**, 67.
Tully, R. B., and Shaya, E. J. 1984, *Ap. J.*, **281**, 31.
van den Bergh, S. 1981, *Ap. J. (Letters)*, **248**, L9.
Visvanathan, N. 1983, *Ap. J.*, **275**, 430.
Vittorio, N., and Silk, J. 1985, *Ap. J. (Letters)*, **293**, L1.
Walker, A. R. 1985, *M.N.R.A.S.*, **212**, 343.
Welch, D. L., McAlary, C. W., McLaren, R. A., and Madore, B. F. 1985, private communication.
Wilkinson, D. T. 1984, in *Large Scale Structure of the Universe, Cosmology and Fundamental Physics*, ed. G. Setti and L. Van Horn (Geneva: CERN), p. 153.
Woody, D. P., and Richards, P. L. 1981, *Ap. J.*, **248**, 18.
Yahil, A., Sandage, A., and Tammann, G. 1977, *Ap. J.*, **217**, 903 (YST).
Zwicky, F., Herzog, E., Wild, P., Karpowicz, E., and Cowal, C. T. 1961–1968, *Catalogue of Galaxies and of Clusters of Galaxies* (6 vols.; Pasadena: California Institute of Technology).

Note added in proof.—The moduli listed in Table 6 are derived by a method equivalent to minimizing the residuals in magnitude. For comparison, an alternative set of moduli were derived by minimizing the residuals in velocity width. The results yielded moduli which averaged 0.01 mag closer, with the largest changes found for Z74-23 (0.04 mag closer) and Pegasus (0.03 mag farther). Given these small differences, it is not surprising that the solar-motion solution of $\Delta V = 760$ km s^{-1} toward $l = 260°$ and $b = 15°$ thereby obtained is in close agreement with the findings in the text.

The revised diamter for UGC 633 (in Pisces) given in Table 2 should be enclosed in parentheses (i.e., it was determined from the correction procedure described in the text and not directly from CCD data).

M. Aaronson and M. E. Cornell: Steward Observatory, University of Arizona, Tucson, AZ 85721

G. Bothun and J. Mould: California Institute of Technology, MS 105-24, Pasadena, CA 91125

J. Huchra: Center for Astrophysics, 60 Garden Street, Cambridge, MA 02138

R. Schommer: Department of Physics and Astronomy, Serin Physics Laboratory, Rutgers University, Piscataway, NJ 08854